Which global reanalysis dataset represents better in snow cover on the Tibetan Plateau?

Shirui Yan[1], Yang Chen[1], Yaliang Hou[1], Kexin Liu[1], Xuejing Li[1], Yuxuan Xing[1], Dongyou Wu[1], Jiecan Cui[2], Yue Zhou[1], Xin Wang[1, *], Wei Pu[1, *]

[1] Key Laboratory for Semi-Arid Climate Change of the Ministry of Education, College of Atmospheric Sciences, Lanzhou University, Lanzhou 730000, China.

[2] Zhejiang Development & Planning Institute, Hangzhou 310030, China.

Correspondence to: Wei Pu, (puwei@lzu.edu.cn); Xin Wang, (wxin@lzu.edu.cn)

Abstract. The extensive snow cover across the Tibetan Plateau (TP) has a major influence on the climate and water supply for over one billion downstream inhabitants. However, an adequate evaluation of Snow Cover Fraction (SCF) variability over the TP simulated by multiple reanalysis datasets has yet to be undertaken. In this study, we used the Snow Property Inversion from Remote Sensing (SPIReS) SCF dataset from the Water Years (WYs) 2001–2017 to evaluate the capabilities of eight reanalysis datasets (HMASR, MERRA2, ERA5, ERA5L, JRA55, CFSR, CRAL, and GLDAS) in simulating the spatial and temporal variability of SCF in the TP. CFSR, GLDAS, CRAL, and ~~The results reveal that~~ HMASR ~~generated~~ are ~~the best~~well in simulating the ~~SCF climatological~~ spatial pattern ~~simulation~~of climatological SCF ~~compared to SPIReS,~~ with lower ~~the least~~ bias and ~~, the~~ higher ~~est~~ correlation ~~coefficient,~~ and ~~the highest~~ Taylor Skill Score (SS) ~~value~~. ~~GLDAS and CFSR also performed well in simulating SCF spatial distribution.~~ In contrast, ERA5L~~,~~ ~~ERA5,~~ ~~and~~ JRA55, and ERA5 ~~showed~~ has relatively good performance in terms of SCF annual trends among eight reanalysis datasets. The biases in SCF simulations across reanalysis datasets are influenced by a combination of meteorological forcings, including snowfall and temperature, as well as the SCF parameterization methods. However, the primary influencing factors vary among the reanalysis datasets. ~~Snow data assimilation and finer resolution could potentially improve SCF simulation accuracy to some extent.~~ Additionally, averaging multiple reanalysis datasets can enhance the spatiotemporal accuracy of SCF simulations, but this enhancement effect does not consistently increase with the number of reanalysis datasets used.

Keywords

Snow cover; Tibetan Plateau; Reanalysis dataset; Meteorological forcing factors; Parameterization methods

1 Introduction

Widespread snow cover on the Tibetan Plateau (TP), with its high albedo and low thermal conductivity, plays a crucial role in the surface energy balance (Zhang, 2005) and affects the climate ~~both~~ locally (Zhang et al., 2022) ~~and~~, across Asia, and globally (Lyu et al., 2018; Ma et al., 2017). Furthermore, in its role as the "Asian water tower" (Kitoh and Arakawa, 2016; Qiu, 2008; Xu et al., 2008), the snow that accumulates on the TP during the cold season is an essential freshwater resource for over a billion people during the warm season, supplying their domestic, agricultural, and industrial water needs (Immerzeel et al., 2010). In the context of climate change, the snow cover over the TP is an extremely sensitive element to warming (Yao et al., ~~2015,~~ 2019; You et al., 2020b). Therefore, the accurate and reliable representation of snow cover over the TP is crucial to regional climate and ecosystem studies.

Comprehensive ground-based measurements face challenges due to ~~Ground-based measurements are the most accurate observations with respect to snow cover (Ma et al., 2022). However, t~~the complex terrain and harsh weather conditions on the TP ~~present challenges to comprehensive monitoring~~ (Yang et al., 2019), leading to issues of spatial representativeness. In contrast, optical satellite observations provide global-scale snow cover data and offer crucial support for snow research. For example, NASA's Moderate Resolution Imaging Spectroradiometer (MODIS) has been providing moderate-resolution global daily snow cover fraction (SCF) data since 2000 (Hall et al., 2002). The Snow Property Inversion from Remote Sensing (SPIReS) then uses a more advanced spectral unmixing technique that provides improvements to SCF estimates for the period Water Years (WYs) 2000–2021 (Bair et al., 2021). However, the more precise satellite products and remote sensing data using more advanced methods have relatively short time spans from 2000 to the present, limiting their role in long-term climate analysis. ~~However, the time period covered by satellite and remote sensing data is relatively short, which limits their utility for long-term climate analysis.~~

Reanalysis methods based on observations and mathematical models (Fujiwara et al., 2017) provide a critical avenue for obtaining long-term snow information~~data~~. These techniques use data assimilation to integrate historical environmental observations with short-term weather

forecasts, yielding optimal estimates of global or regional weather and climate states (Lei et al., 2023). In recent decades, the major meteorological agencies around the world have generated atmospheric and land reanalysis products at varying temporal and spatial resolutions (Fujiwara et al., 2017). Reanalysis datasets have become indispensable sources of data when it comes to studying processes related to snow variability, as well as their impacts and responses to climate change (Lin and Wu, 2011; Thackeray et al., 2016; Wegmann et al., 2017). For example, the reanalysis snow dataset (e.g., ERA40 and NCEP-NCAR) has revealed that anomalous snow cover in prior autumn facilitates a warm-north, cold-south winter over North America by influencing the teleconnection response in the Pacific-North American (PNA) region (Lin and Wu, 2011). Reanalysis datasets (e.g., MERRA, ERA-Interim, and GLDAS-2) have been integrated into the Canadian Sea Ice and Snow Evolution (CanSISE) dataset to analyze the impacts of global warming on snow changes on the TP (You et al., 2020a).

A comprehensive evaluation of multiple snow reanalysis datasets based on referenced observation data is of paramount importance before launching related scientific research. Previous researches have focused more on the accuracy of ~~has devoted considerable attention to evaluating~~ Snow Depth (SD) and Snow Water Equivalent (SWE) in reanalysis datasets ~~using various metrics from~~across different regions (Bian et al., 2019; Li et al., 2022; Wang and Zeng, 2012; Zhang et al., 2021). However, only Orsolini et al. (2019) and Li et al. (2022) ~~a few studies~~ have assessed the SCF performance of reanalysis datasets over the High Mountain Asia ~~TP~~ based on SCF data from the Interactive Multisensor Snow and Ice Mapping System (IMS; Helfrich et al., 2007) and ground observations ~~(Li et al., 2022; Orsolini et al., 2019)~~. ~~These~~ Their studies considered the SCF accuracy of ~~have provided comparisons of the SCF spatial patterns among~~ a limited number of reanalysis datasets~~, and they~~ and lacked multidimensional evaluation ~~analysis~~ that considers aspects such as regional variations and annual trends ~~(Li et al., 2022; Orsolini et al., 2019)~~, as well as an in-depth analysis of the impact of parameterization on SCF bias. In addition, the IMS dataset, which uses microwave remote sensing technology, is challenging for detecting shallow or wet snow that may lead to increased uncertainty in SCF detection (Yu et al., 2013). ~~The discussion by Li et al. (2022) on the simulation errors of SCF~~

~~in reanalysis datasets appears somewhat lacking.~~ Therefore, prior evaluations of reanalysis SCF datasets are still insufficient.

The various reanalysis snow datasets have unique spatiotemporal characteristics (Mudryk et al., 2015). The differences in snow characteristics originate not only from the use of different Land Surface Models (LSMs), but also from the meteorological forcing data and parameterization methods~~post-optimization via snow data assimilation~~. De Rosnay et al. (2014) indicated that the accuracy of snow simulations is constrained largely by uncertainties associated with some of the key meteorological inputs, including precipitation and temperature (Cao et al., 2020; Zhang et al., 2015), under regional climate conditions and elevation factors (Brown and Mote, 2009; Hernández-Henríquez et al., 2015). Therefore, uncertainties associated with precipitation and temperature data are likely to be the primary sources of bias within the reanalysis SCF datasets. Moreover, Jiang et al. (2020) emphasized that optimizing the parameterization methods used to convert SD or SWE to SCF ~~for SCF calculation~~ would reduce the uncertainties associated with snow modeling, which would further reduce biases in land surface albedo simulations, particularly in high-altitude regions. The reanalysis datasets use different SCF parameterization methods, with a 100% SCF corresponding to an SD that ranges from 2 to 26 cm (Orsolini et al., 2019). The selection of different SCF parameterizations for the reanalysis datasets may lead to varying degrees bias of SCF. ~~On the other hand, data assimilation represents an effective approach to reducing the uncertainties in snow models and enhancing the ability to monitor seasonal snow changes (Andreadis and Lettenmaier, 2006; Sun et al., 2004). Brown et al. (2003) used optimal interpolation (OI) techniques to assimilate SD observations, resulting in gridded monthly SD and SWE datasets that were better aligned with in situ and satellite data across North America.~~

For this study, we conducted an in-depth evaluation of SCF simulations derived from eight atmospheric and land assimilation reanalysis datasets over the period ~~Water Years (~~WYs~~)~~ 2001–2017, using SPIReS SCF dataset ~~data~~ as a reference. The accuracy of SCF was assessed multidimensionally by examining the spatial characteristics, seasonal variations, and annual trends across the whole TP and its nine basins. Additionally, we aimed to assess the influence

of meteorological forcing ~~factors~~ (snowfall and temperature)~~,~~ and the SCF parameterization ~~methods, and snow assimilation~~ on the SCF biases associated with the various reanalysis datasets. On this basis, we attempted to develop an optimal combination of reanalysis SCF datasets ~~and provide a useful guide for the research community regarding climatic and cryospheric changes over the TP~~.

2 Data and methods

2.1 Data

2.1.1 Remote sensing data

For this study, we utilized the SPIReS SCF dataset ~~data~~ (Bair et al., 2021) as the reference SCF ~~data~~. It is derived from Landsat 8 Operational Land Imager (OLI) and MODIS data using a spectral unmixing methodology at a 4 km resolution for the period spanning WY 2000 to WY 2021 (e.g., WY 2000 refers to October 1, 1999, to September 30, 2000). The SCF calculation in SPIReS relies on two endmembers (i.e., snow and snow-free) along with an ideal shade component, effectively simplifying the calculation process while maintaining high accuracy. SPIReS reduces the effects of cloud noise through interpolation and smoothing to provide more accurate SCF data (Bair et al., 2021; Dozier et al., 2008). In a comprehensive evaluation conducted by Stillinger et al. (2023) utilizing airborne lidar datasets for subcanopy snow mapping performance over mountain areas in the western United States, spectral unmixing-derived data (including SPIReS and MODIS Snow-Covered Area and Grain Size, abbreviated as MODSCAG) exhibited lower bias and Root Mean Square Error (RMSE) compared to data derived from band ratio methods and spectral mixture methods. Moreover, unlike MODSCAG, SPIReS incorporates the influence of light-absorbing particles on snow, leading to more accurate SCF data.

2.1.2 Reanalysis datasets

We examined eight widely used reanalysis datasets obtained from various meteorological

organizations, with details listed in Table 1. Meteorological forcing fields are used to drive the LSMs, and parameterization methods are used to calculate the daily SCF data. ~~However, t~~The assimilation of snow data varied among the datasets.

The High Mountain Asia Snow Reanalysis (HMASR; Liu et al., 2021) is a snowpack-specific reanalysis dataset produced by NASA High Mountain Asia Team (HiMAT). HMASR uses the Simplified Simple Biosphere model, version 3 (SSiB3; Sun and Xue, 2001; Xue et al., 2003) as the LSM to generate the initial snowpack mass for WYs 2000–2017 based on meteorological inputs from MERRA2 and physiographic characteristics. The model-derived SCF predictions are then constrained by integrating spectral unmixing algorithm derived SCF data from the MODIS and Landsat satellites products (Painter et al., 2009) via data assimilation. The parameterization method used in HMASR (abbreviated as SSiB3_SCF in Table 1) has not been publicly disclosed.

The Modern-Era Retrospective analysis for Research and Applications, version 2 (MERRA2; Gelaro et al., 2017)~~ dataset~~, developed by NASA's Global Modeling and Assimilation Office (GMAO), provides land surface state estimates including SCF via the Catchment LSM (CLSM; Koster et al., 2000). The surface-forced precipitation is a combination of the National Oceanic and Atmospheric Administration (NOAA) Climate Prediction Center (CPC) unified gauge-based analysis of global daily precipitation (CPCU; Xie et al., 2007) product and the precipitation generated by the atmospheric general circulation model within the MERRA2 system. The generated precipitation is also adjusted using a precipitation correction algorithm (Reichle et al., 2017). ~~However, it is important to note that~~ MERRA2 does not include snow data assimilation. The parameterization scheme in MERRA2 considers 100% SCF to occur when the SWE reaches a threshold of 26 kg m^{-2} (abbreviated as MM_SCF in Table 1; Orsolini et al., 2019; Reichle et al., 2017).

The ECMWF Reanalysis version 5 (ERA5; Hersbach et al., 2020), produced and published by the European Centre for Medium-Range Weather Forecasts (ECMWF), uses the Tiled ECMWF Scheme for Surface Exchanges over Land (HTESSEL) model to simulate various land surface variables~~ including SCF~~. The precipitation forcing in ERA5 is adjusted using

Global Precipitation Climatology Project (GPCP; Adler et al., 2003) data. ERA5 assimilates in situ SD observations and binary SCF data from IMS only below 1500 m, so that snow assimilation does not apply to the TP region (Bian et al., 2019). Additionally, a refined dataset known as ERA5-Land (abbreviated as ERAL; Muñoz-Sabater et al., 2021) has been derived from ERA5 via the offline rerunning of the land portion of the model at a higher spatial resolution. ERA5L provides solely land surface parameters and is based on the same forcing and LSM as ERA5. Both datasets have a 10-cm SD threshold to identify full SCF (abbreviated as ME_SCF in Table 1; ECMWF, 2018; Orsolini et al., 2019). ERA5 does not directly output the SCF variable. The SCF values for ERA5 used in this study was calculated using ME_SCF method.

The Japanese 55-year Reanalysis (JRA55; Kobayashi et al., 2015), developed by the Japan Meteorological Agency (JMA), generates the land surface analysis field using an offline version of the Simple Biosphere (SIB) model (Sato et al., 1989; Sellers et al., 1986). The precipitation forcing is corrected using precipitable water retrieved from the Special Sensor Microwave/Imager (SSM/I) brightness temperature (Onogi et al., 2007). JRA55 incorporates daily SD data from the SSM/I and the Special Sensor Microwave Imager Sounder (SSMIS) using a univariate two-dimensional optimal interpolation (OI) ~~OI~~ approach. In addition, it assimilates surface synoptic observations (SYNOP) reports and digitizes China's daily SD data from 1971 to 2006 (Onogi et al., 2007). The detection of full SCF in JRA55 is based on a 2-cm SD threshold (abbreviated as MJ_SCF in Table 1; Orsolini et al., 2019). Similar to ERA5, the SCF in JRA55 was also calculated rather than provided directly by the product.

The Climate Forecast System Reanalysis (CFSR; Saha et al., 2010), developed by the National Center for Environmental Prediction (NCEP) under NOAA, is a weakly coupled global reanalysis system. The land surface analysis utilizes the Noah model (Meng et al., 2012). Two observed global precipitation analyses, namely the CPC Merged Analysis of Precipitation (CMAP; Xie and Arkin, 1997) and the CPCU, are used as alternative forcings for precipitation. In terms of snow analysis, CFSR assimilates IMS and the Global Snow Depth Model (SNODEP). On 1 January 2011, CFSR transitioned to a newer version of the NCEP data

assimilation system called CFSv2 (Saha et al., 2014). Despite differences in horizontal resolution and minor changes to the physical parameterization, CFSv2 is considered a continuation of CFSR in most cases (Fujiwara et al., 2017). The SCF parameterization method in CFSR is related to the surface characteristics, using varying SD thresholds to identify the full SCF depending on the underlying surface type (abbreviated as Noah_SCF in Table 1; Ek et al., 2003).

The Global Land Data Assimilation System version 2.1 (GLDAS-2.1; Rodell et al., 2004) is a global land data assimilation product developed jointly by NASA and NOAA. It uses the global meteorological forcing dataset from Princeton University (Sheffield et al., 2006) and the GPCP V1.3 Daily Analysis precipitation fields (Adler et al., 2003; Huffman et al., 2001) to drive three distinct LSMs: the CLSM model, the Noah model, and the Variable Infiltration Capacity (VIC) model. As a result, four datasets are generated (Table S1). Notably, the full series datasets within GLDAS-2.1 do not assimilate snow observations. Furthermore, owing to the unavailability of SCF variables in these datasets, this study derived different SCF values using three parameterization methods (MM_SCF, ME_SCF and MJ_SCF). Finally, the 0.25° × 0.25° GLDAS–Noah product using the MM_SCF approach was selected as a representative of GLDAS due to its better SCF simulation (Fig. S1).

China's First Generation Global Atmospheric and Land Reanalysis (CRA-40; Liu et al., 2023) is produced by the China Meteorological Administration (CMA). The matched land surface reanalysis datasets (CRA-40/Land, abbreviated as CRAL) are simultaneously generated offline based on an updated version of the Noah model and atmospheric driving factors from CRA-40. In CRAL, precipitation meteorological forcing is derived from a similar combination of data sources as CFSR (Liang et al., 2020). ~~However,~~ CRAL does not assimilate other observational data in the LSM. Instead, data from over 2,400 CMA surface weather observatories indirectly influence the land surface product through conventional meteorological forcing derived from atmospheric reanalysis (Liang et al., 2020). The SCF parameterization method in CRAL is the same as that in CFSR.

Table 1: Characteristics of the reanalysis datasets used in this study.

Reanalysis dataset	Agency ~~Centre~~	Temporal coverage	Resolution	Land Model	Snow data assimilation	Variables used in analysis [b]	SCF parameterization method used in this study	Reference dataset
HMASR	NASA ~~HIMAT~~HiMAT	WY 1999 to WY 2017	1/225°×1/225°	SSiB3	MODIS and Landsat	SCF, SWE, SD	SSiB3_SCF	Liu et al., (2021)
MERRA2	NASA GMAO	1980 to present	0.625°×0.5°	Catchment	-	SCF, SWE, SD, T2, Snowfall	SCF= min (1, SWE/26) [a]	Gelaro et al., (2017)
ERA5	ECMWF	1979 to present	0.25°×0.25°	H-TESSEL	-	SWE, SD, T2, Snowfall, RH	SCF= min (1, (SD)/10) [a]	Hersbach et al., (2020)
ERA5L	ECMWF	1981 to present	0.1°×0.1°	H-TESSEL	-	SCF, SWE, SD, T2, Snowfall	SCF= min (1, (SD)/10) [a]	Muñoz-Sabater et al., (2021)
CRAL	CMA	1979 to present	0.5°×0.5°	Noah	-	SCF, SWE, SD, T2, Snowfall	Noah_SCF	Liu et al., (2023)
JRA55	JMA	1958 to present	0.563°×0.563°	SiB	Station, SSM/I, SSMIS	SWE, SD, T2, Snowfall	SCF= min (1, (SD)/2) [a]	Kobayashi et al., (2015)
CFSR	NOAA NCEP	1979 to present	0.5°×0.5°	Noah	SNODEP, IMS	SCF, SWE, SD, T2, Snowfall	Noah_SCF	Saha et al., (2010); Saha et al., (2014)
GLDAS	NASA and NOAA	2000 to present	0.25°×0.25°	Noah	-	SWE, SD, T2, Snowfall	~~Noah~~MM_SCF	Rodell et al., (2004)

[a] The unit for SWE is kg m^{-2}, and for SD is cm. [b] ERA5, ~~and~~ JRA55, and GLDAS do not provide output for the SCF variable directly. In this study, the SCF values for ERA5 and JRA55 were derived using their respective parameterization methods, as shown in the Table 1. The SCF values for GLDAS were derived using MERRA2 parameterization methods. ~~as shown in the Table 1.~~ T2 is 2-m air temperature.

2.1.3 Meteorological dataset

To investigate the effects of snowfall and temperature biases on SCF bias, we used precipitation and 2-m air temperature data from the high-resolution near-surface Meteorological Forcing Dataset for the Third Pole region (TPMFD; Yang et al., 2023) as the reference data. Precipitation and 2-m air temperature in TPMFD were derived by combining a short-term high-resolution Weather Research and Forecasting (WRF) simulation (Zhou et al., 2021), long-term ERA5 data, and in situ observations, all at a resolution of 1/30° for the period spanning 1979 to 2020. Validation conducted by Jiang et al. (2023) demonstrated that the precipitation data from TPMFD are unbiased overall and considerably better than other widely used datasets~~, including the latest generation of reanalysis (ERA5L), a state-of-the-art satellite-based dataset (the Integrated Multi-satellitE Retrievals for Global Precipitation Measurement, abbreviated as~~

~~IMERG), and multi-source merged datasets (the Multi-Source Weighted-Ensemble Precipitation version 2, abbreviated as MSWEP v2, and the long-term Asian precipitation dataset, abbreviated as AERA5-Asia)~~. To obtain snowfall data for ~~our~~ this study, we applied a dynamic threshold parameterization scheme, which considers surface air conditions such as wet bulb temperature, altitude~~surface elevation~~, and relative humidity, to convert TPMFD total precipitation to snowfall~~to convert precipitation data in TPMFD to snowfall~~. This approach has been proven effective in capturing snowfall variations on the TP through comparisons with station observations (Ding et al., 2014) and has been used in many studies (Deng et al., 2017; Luo et al., 2020; Yang et al., 2021; Zhu et al., 2021). For detailed calculation methods and further information, readers are referred to the work of Ding et al. (2014). We note that TPMFD lacks the relative humidity variable necessary for snowfall conversion, while all variables in TPMFD are assimilated from ERA5 data. Therefore, we utilized ERA5 surface relative humidity as a substitute.

2.2 Study region

The boundary of the TP used in this study is identified as an isoline of 2,500 m according to the Global Multi-resolution Terrain Elevation Data 2010 (Danielson and Gesch, 2011), spanning from 26°N to 41°N and from 67°E to 105°E (Fig. 1b). The prevailing westerlies and monsoons are the primary moisture sources in this region, exerting significant influence on the spatial and temporal distribution of snowfall and glacier mass balance (Liu et al., 2021; Yao et al., 2012). Specifically, the westerlies dominate winter precipitation, while the Indian and East Asian monsoons dominate summer precipitation in the southeast (Yao et al., 2012), resulting in diverse snow regimes. We identified nine major river basins within the TP using Hydrological Data and Maps Based on Shuttle Elevation Derivatives at Multiple Scales (HydroSHEDS; Lehner et al., 2008), namely the Amu, Indus, Tarim, Inner Tibetan Plateau (~~abbreviated as~~ ITP), Brahmaputra, Salween, Mekong, Yangtze, and Yellow basins. Due to the differing impacts of winter and summer atmospheric forcing, the performance of SCF simulations from reanalysis datasets varies across these basins.

2.3 Methods

2.3.1 Evaluation of SCF accuracy for reanalysis datasets

In this study, we used time series spanning from WYs 2001–2017, covering periods for which all data were available. Before ~~our~~ evaluation, all data were regridded to a 0.5°×0.5° grid via ~~via the~~ bilinear interpolation for MERRA2, JRA55, and CRAL, and the grid averaging approach for HMASR, ERA5, ERA5L, GLDAS, SPIReS, and TPMFD.~~method to 0.5°×0.5° grids, ensuring the resolution uniformity between different datasets. After unifying the resolution, all datasets included 1200 pixel points in the TP.~~

For each 0.5°×0.5° grid cell within the TP, we calculated the climatological SCF over the full period and seasonally for SPIReS and eight reanalysis datasets (e.g., Fig. 1a and Fig. S3). Absolute bias and correlation (Pearson's correlation coefficient) were calculated from these values at both the basin and the TP scales. Spatial distribution and basin-averaged values of the climatological SCF, as well as bias maps of the reanalysis datasets compared to SPIReS, are presented. Additionally, Taylor diagrams are used to provide additional information regarding the RMSE and standard deviation ratio (STDR). The climatological SCF values for each grid cell within basin and region were used as input to calculate the Taylor Diagram's component metrics (correlation, RMSE, and STDR). The component metrics were summarized by the Taylor Skill Score (SS) as follows:

~~We employed absolute bias and Pearson's correlation coefficient (R) as the evaluation metrics for assessing SCF accuracy. To visually capture the spatial variability of SCF climatology across multiple dimensions in the reanalysis datasets, Taylor diagrams (Taylor, 2001) were further employed to represent the combined information of R, RMSE, and Standard Deviation Ratio (STDR). These three metrics in the Taylor diagrams of Fig. 2b were computed for 1200 pixel points within the TP between reanalysis datasets and SPIReS after averaging the SCF climatology from WY 2001 to WY 2017. R and RMSE describe the degree of phase and amplitude agreement of the reanalysis SCF climatological spatial fields with SPIReS. To facilitate comparison across reanalysis datasets in one Taylor diagram, we normalized the~~

~~Standard Deviation (STD) to obtain STDR, representing the consistency in dispersion of spatial field values between reanalysis datasets and SPIReS (Cui et al., 2021). Better performance is indicated by relatively higher R, lower RMSE, and closer STD (in other words, STDR closer to 1). Additionally, Taylor Skill Scores (SS, ranging from 0 to 1; Taylor, 2001) were calculated to provide comprehensive statistics for the composite index. The SS is defined as follows:~~

$$SS=\frac{4(1+R)^4}{(STDR+1/STDR)^2(1+R_0)^4} \quad (1)$$

where R_0 is the maximum correlation attainable. ~~The R and RMSE required to calculate SS in Fig. 4 are consistent with the method described above, but for different seasonal averages for SCF climatology.~~

The ~~reliability of annual trend analysis depends on the significance testing, and the sign (+ or –) may impact the robustness of the annual trend analysis results. Therefore, we used the~~ Mann-Kendall (MK; Kendall, 1975; Mann, 1945) test was used to assess ~~to ascertain~~ the significance of annual trends~~,~~. Since the sign (+ or –) may impact the robustness of the trend analysis results, we employed ~~and~~ the Consistency Index (CI; Zhang et al., 2021) to compare the agreement in SCF annual trend signs between the reanalysis datasets and SPIReS. The CI is defined as follows: ~~to validate the SCF annual trends. The CI is defined as follows:~~

$$CI=\frac{N_{inc}+N_{dec}+N_{no}}{N_{tot}} \quad (2)$$

where N_{inc} is the number of grid points with a significant increasing trend in both the reanalysis dataset and SPIReS ($P < 0.05$), N_{dec} is the number of grid points with a significant decreasing trend in both datasets, N_{no} is the number of grid points with a non-significant trend in both datasets, and N_{tot} is the total number of grid points. The higher the CI value, the better the performance of the trend simulation.

~~2.3.2 Analysis of SCF bias sources and generation of optimal datasets~~

2.3.2 Analysis of SCF bias sources for meteorological forcings

Variations in snowfall and temperature are the dominant influences on snow evolution and can explain half to two-thirds of the interannual variability in snow cover (Xu et al., 2017). Hence, biases in snowfall and temperature within reanalysis datasets are likely the main sources of bias

in SCF. Here, the analysis of bias sources was primarily based on correlation analysis between the bias of SCF and those of snowfall and temperature. ~~Similar to the SCF case, t~~The absolute biases of snowfall and temperature were computed by comparing the reanalysis datasets with TPMFD. Additionally, we calculated the correlation ~~R~~ between the annual time series of snowfall and temperature ~~annual average~~ biases ~~in snowfall and temperature~~ at each TP grid cell ~~pixel point over the TP~~ and SCF ~~SCF~~ bias~~es~~ ~~–~~to obtain the spatial distribution of correlations as shown in Fig. ~~3~~6.

2.3.3 Analysis of SCF bias sources for parameterization method

Evaluations have shown that in the TP, with relatively thin and short-lived snow (Huang et al., 2023), ~~In the snow model,~~ optimizing the SCF parameterization ~~method~~ can significantly reduce the annual SCF bias~~es~~ in snow models (Jiang et al., 2020). Orsolini et al. (2019) noted that SCF parameterization differs significantly among reanalyses, affecting SCF bias. For the eight reanalysis datasets considered here, five parameterizations ~~methods~~ were used to convert SWE or SD into SCF; i.e., MM_SCF, ME_SCF, MJ_SCF, SSiB3_SCF, and Noah_SCF (see Section 2.1.2 and Table 1). ~~These parameterization methods have been evaluated in diverse regions (Orsolini et al., 2019), and the results indicate that different parameterizations of snow processes will introduce different uncertainties into snow simulations (Jiang et al., 2020). Moreover, specific challenges arise on the TP because of its complex terrain and unstable snow conditions (Huang et al., 2023).~~ In order to evaluate the impact of the parameterization ~~method~~ on SCF simulations, we incorporated three publicly available and easily offline-usable parameterization methods (MM_SCF, ME_SCF, and MJ_SCF) separately into each reanalysis dataset. For HMASR, CRAL, and CFSR, which do not include their parameterization among these three methods, we derived three additional SCF datasets. MERRA2, ERA5, ERA5L, JRA55, and GLDAS ~~to~~ derive another ~~three (~~two SCF datasets~~) SCF products for HMASR, CRAL, and CFSR (MERRA2, ERA5, ERA5L, JRA55, and GLDAS)~~.

2.3.4 Generation of combined optimal datasets

Mortimer et al. (2020) demonstrated that product accuracy can be enhanced by averaging multiple reanalysis datasets, as this allows unrelated errors and deficiencies between them to offset each other. To investigate whether averaging of multiple datasets can improve SCF accuracy over the complex terrain of the TP, we considered all possible combinations of the eight reanalysis datasets, totaling 247. The output of each combined dataset was computed as the equally weighted average of all reanalysis datasets in the combination (Mudryk et al., 2015). Subsequently, we characterized the SCF accuracy of combined datasets in spatial distribution and annual trends by computing the SS and CI values.

3. Results

3.1 Evaluation of spatial and temporal accuracy in SCF~~Spatial variability of SCF climatology~~

3.1.1 Spatial variability of SCF climatology ~~Evaluation of spatial variability~~and seasonality

~~The reanalysis datasets exhibit a range of SCF patterns over the TP (Fig. 1a). The basin-averaged values were obtained by averaging pixel points within each basin of the TP after SCF climatological average from WY 2001 to WY 2017 (Fig. 1b).~~ The ~~TP~~ TP-averaged ~~of~~ SCF ~~climatology from~~ for HMASR, GLDAS, and CRAL ~~are~~ is 0.14, 0.12, and 0.12, respectively, which align closely with the SPIReS value of 0.13 (Fig. 1b). ~~In more detail,~~ HMASR (GLDAS and CRAL) ~~displays a~~ slightly ~~underestimation~~ underestimates (~~overestimation~~overestimate) in westerlies-dominated basins such as the Amu and Indus, and ~~overestimation~~ overestimates (~~underestimation~~underestimate) in monsoon-dominated basins such as the Yellow, Yangtze, Mekong, Salween, and Brahmaputra (Fig. 2a). These regional biases average out when considering the entire TP, which is reflected in the strong permanence of these datasets over the TP.~~These biases probably average out when looking at the TP as a whole, resulting in more~~

~~accurate reanalysis SCF simulations.~~ Conversely, ~~On the other hand,~~ ERA5, ERA5L, and JRA55 have ~~show~~ large positive SCF biases across all basins, whereas MERRA2 has ~~displays~~ a ~~large~~ negative bias ~~in SCF~~ in all basins.~~.~~ Over the TP as a whole, ERA5 (MERRA2) has the largest positive (negative) bias~~In comparison to SPIReS, ERA5 stands out as the dataset showing the highest positive bias, while MERRA2 demonstrates the largest negative bias, with extreme TP average values of 0.41 and 0.05, respectively (Fig. 1b)~~.

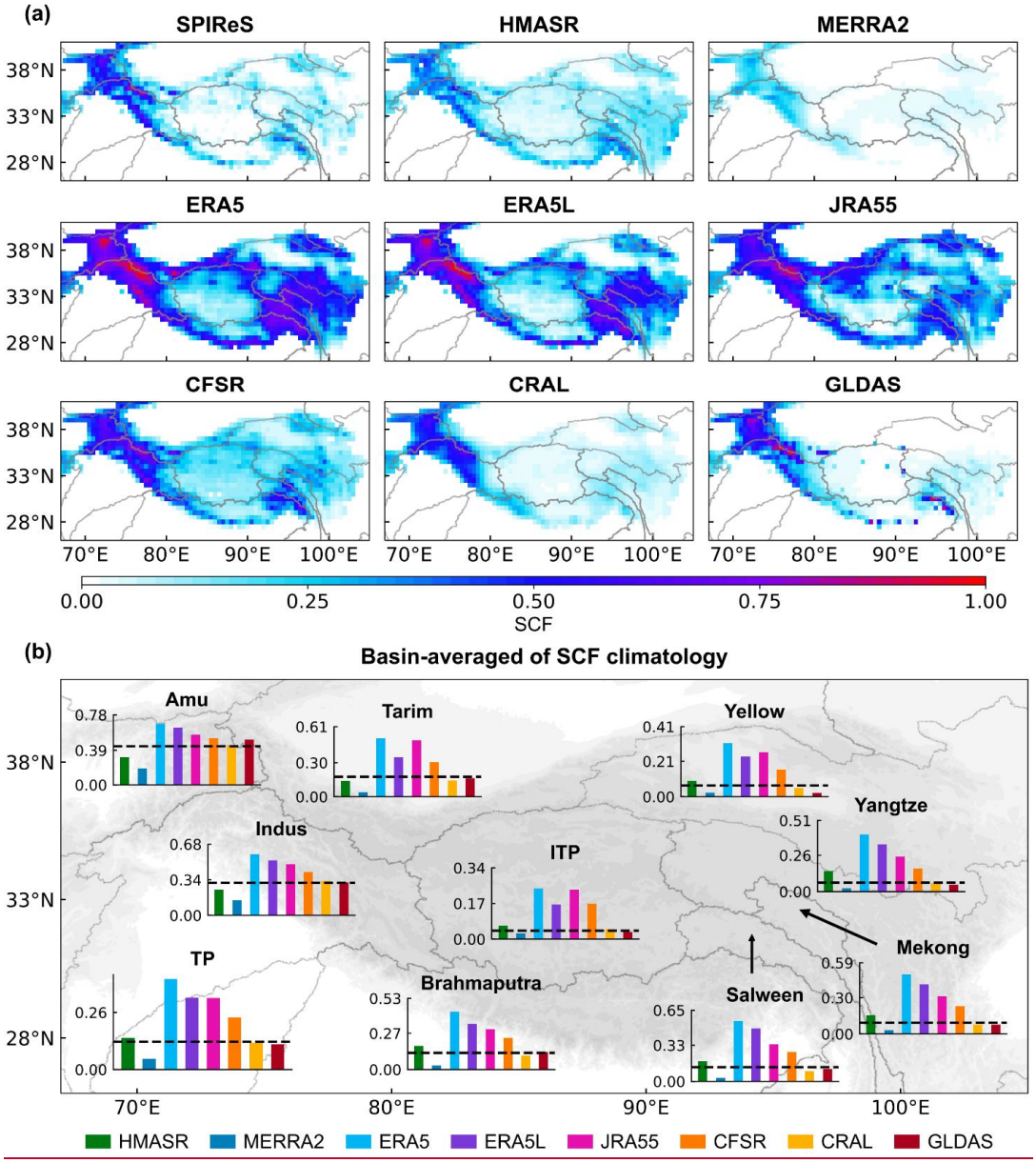

Figure 1: (a) Spatial distribution of Snow Cover Fraction (SCF) climatological average for Water Years (WYs) 2001–2017 from SPIReS and eight reanalysis datasets over the Tibetan Plateau region. (b) Basin-averaged of SCF climatology from SPIReS (black horizontal line) and the eight reanalysis datasets overlain on a map of the TP. ITP = Inner Tibetan Plateau.

All datasets have similar spatial patterns of SCF, with higher values in the western TP and lower values in the interior (Fig. 1a). However, compared to SPIReS, the magnitude and sign of their biases vary spatially (Fig. 2a). This variation is demonstrated by their differing correlation, STDR, and RMSE values (Fig. 2b; see Fig. S2 for a clearer version) and hence their SS values(Fig. 2c) between the reanalysis datasets and SPIReS.~~Figures 1a and 2a further show that, although all reanalysis datasets have spatial SCF patterns that are similar to those from SPIReS, the varying magnitude of SCF value across these datasets results in different correlations (characterized by R values), bias (characterized by RMSE values) and similarities in dispersion patterns (characterized by STDR values) when compared with SPIReS, which ultimately influences their synthesis performance (characterized by SS values). In the Taylor diagram (Fig. 2b; see Fig. S2 for a clearer version), HMASR~~CFSR has the highest SS ~~R~~ value~~s~~ of 0.83, reflecting its strong correlation in ~~across~~ westerlies-dominated basins and variability close to that of SPIReS in monsoon-dominated basins (STDR close to 1, e.g., 0.98 for the Indus basin)~~all basins, with STDR values for monsoon-dominated basins close to 1 (e.g., 1.01 for the Salween basin)~~. The SS values for GLDAS, CRAL, and HMASR are all above 0.7, benefiting from their high correlations similar to CFSR. Consequently, these four datasets ~~HMASR~~ have ~~achieves the highest SS value of 0.68, indicating its~~ superior SCF spatial performance across the TP. In contrast, although ~~Following HMASR, GLDAS comes next, with its R values ranking second in the TP. Meanwhile, GLDAS captures high SCF climatological values in the Tarim and Indus basins and low values in the ITP, Yellow, and central Brahmaputra basins, similar to SPIReS (Fig. 1a), giving it better STDR values in the TP compared to HMASR (Fig. 2b). CFSR consistently exhibits high R values across all basins, despite its positive bias in the TP average of SCF climatology. Consequently, CFSR has an SS value of 0.57, similar to GLDAS. In contrast to CFSR, although CRAL has a TP average close to SPIReS, its spatial distribution is overly uniform, with a relatively low R value and high RMSE, leading to a moderate SS value. Other reanalysis datasets that overestimate SCF climatology, such as~~ ERA5, ERA5L, and JRA55~~,~~ can adequately ~~are able to~~ capture the STDR ~~well~~ in monsoon-dominated ~~some~~ basins, ~~but~~ their large positive biases lead to ~~result in~~ high RMSE, resulting in moderate ~~and low~~ SS

values across ~~in~~ the TP~~, consistent with Bian et al. (2019)~~. MERRA2 has the worst spatial performance, with the lowest SS value in all basins and across the TP~~shows the worst STDR and SS value, not only across the TP but also within each basin~~. This contradicts ~~. This seems opposite to the conclusions of~~ Orsolini et al. (2019),~~,~~ who found MERRA2 to perform well in capturing the SCF and ~~SWE~~ SD characteristics ~~on the TP~~. T~~he reason for t~~his discrepancy arises because ~~is that~~ their results depended mainly on the high correlation between MERRA2 and the reference dataset, ignoring ~~while overlooking the~~ severe underestimations in SCF values. These underestimations result in ~~a~~ very small self-standard deviations ~~STD~~ in the STDR calculation, leading to the lowest ~~worst~~ SS value ~~in this study of 0.16.~~.

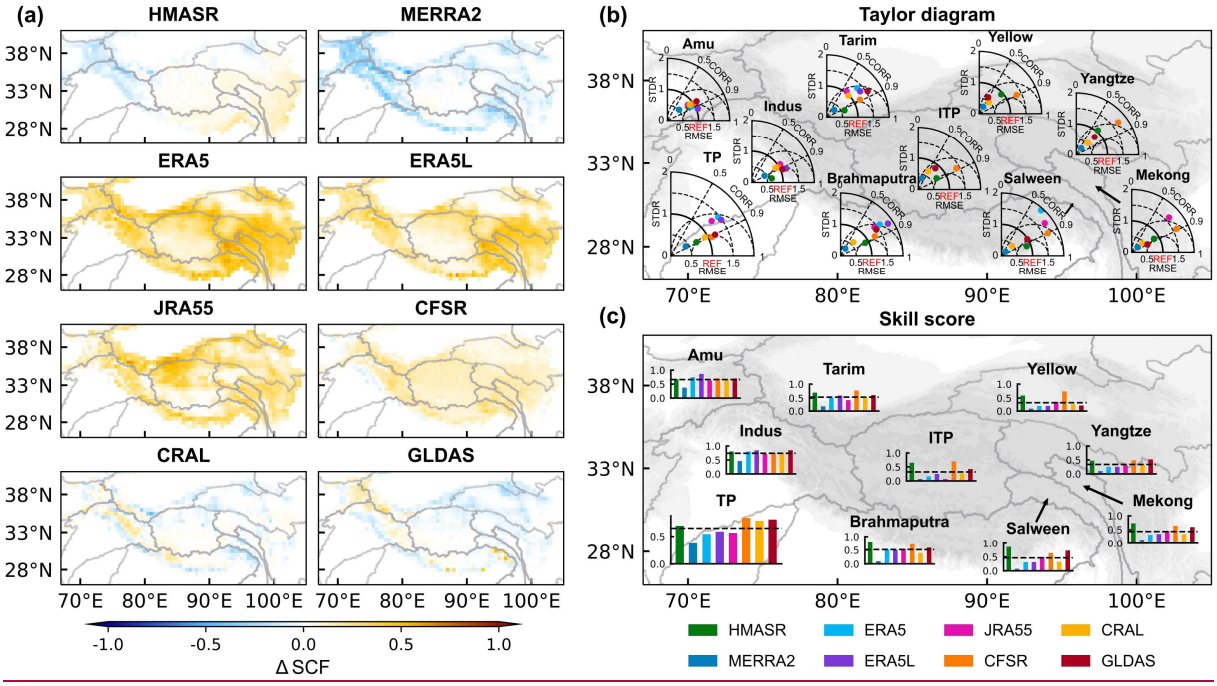

Figure 2: (a) Spatial distribution of the SCF climatological bias from the reanalysis datasets based on SPIReS over the TP. (b) Taylor diagrams showing the correlation coefficients (R), Root Mean Square Error (RMSE), and Standard Deviation Ratio (STDR) of SCF between reanalysis datasets and SPIReS for each basin, overlain on a map of the TP. (c) Taylor Skill Scores (SS) for each basin overlain on a map of the TP. The black line is the average of the SS values for all reanalysis datasets in basin.

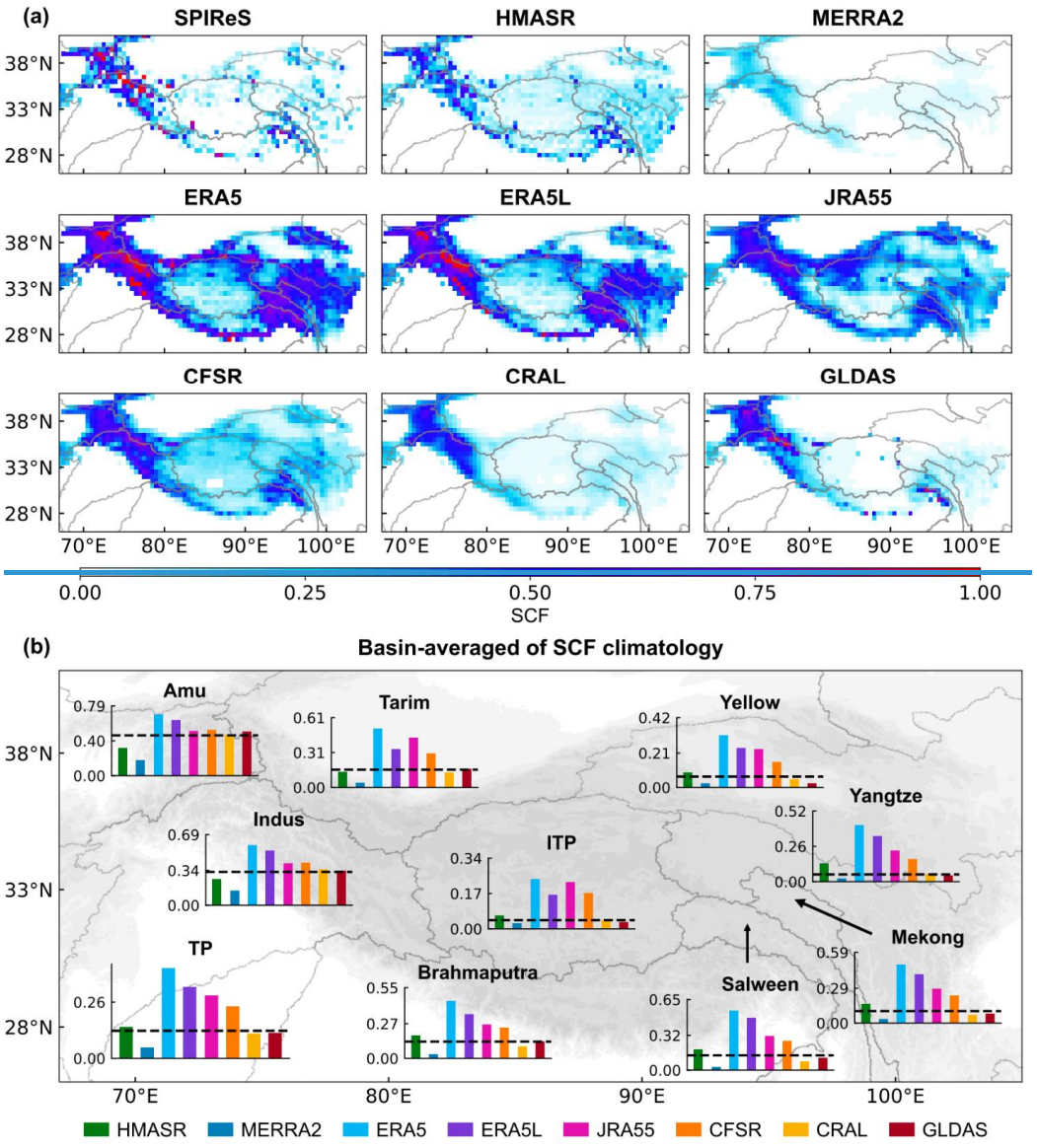

~~**Figure 1: (a) Spatial distribution of Snow Cover Fraction (SCF) climatological average for Water Years (WYs) 2001–2017 from SPIReS and eight reanalysis datasets over the Tibetan Plateau region. (b) Basin-averaged of SCF climatology from SPIReS (black horizontal line) and the eight reanalysis datasets overlain on a map of the TP. ITP = Inner Tibetan Plateau.**~~

~~For each reanalysis dataset, the SCF simulation exhibits varying spatial performance over different TP basins, influenced by their unique topographic and climatic characteristics.~~ Basins affected primarily by the winter westerlies (e.g., the Amu and Indus basins) have better spatial performance, ~~display better consistency between~~with the SS values for all reanalysis datasets within these basins exceeding 0.66 (Fig. 2c) ~~reanalysis datasets and SPIReS~~. ~~The Indus basin shows the best SCF spatial performance with the highest SS value (Fig. 2c).~~ In basins influenced by the summer monsoon (e.g., the Yellow, Yangtze, Mekong, Salween, and Brahmaputra basins),

SCF spatial consistency with SPIReS ~~performance~~ varies. The basin-averaged of SCF climatology is highly biased in the Yellow and Yangtze basins for ~~the~~ reanalysis datasets (Fig. 1b). Specifically, the basin-averaged SCF ~~climatological basin-averaged~~ values of ERA5, ERA5L, and JRA55 (MERRA2) are more than 2× larger (lower) than SPIReS. These biases result in varied RMSE and STDR among these reanalysis datasets (Fig. 2b) and lower SS values (Fig. 2c). However, this phenomenon is less pronounced in the Salween and Brahmaputra basins~~, where SS values are relatively higher~~. The Tarim and ITP basins are considered inland basins. In particular, the ITP basin shows the poorest SCF spatial performance among basins, with the reanalysis average SS values ~~of the reanalysis datasets <~~only 0.~~15~~33~~, except for HMASR~~.

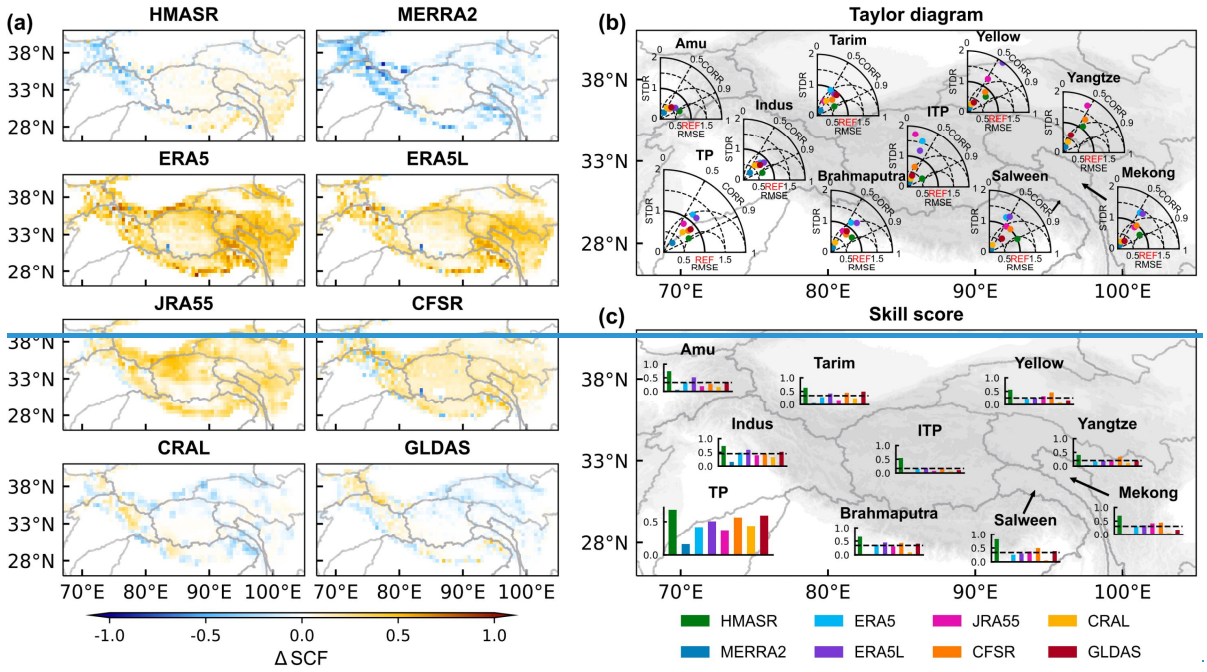

~~Figure 2: (a) Spatial distribution of the SCF climatological bias from the reanalysis datasets based on SPIReS over the TP. (b) Taylor diagrams showing the correlation coefficients (R), Root Mean Square Error (RMSE), and Standard Deviation Ratio (STDR) of SCF between reanalysis datasets and SPIReS for each basin, overlain on a map of the TP. (c) Taylor Skill Scores (SS) for each basin overlain on a map of the TP. The black line is the average of the SS values for all reanalysis datasets in basin.~~3.1.2 ~~Spatial variability of seasonal SCF~~

Figure 3 shows the SCF bias, its probability density distribution, and the SS values for four seasons. In general, the different seasons have similar spatial patterns of SCF bias for each

reanalysis dataset (Fig. 3, first to fourth columns on left). However, there are seasonal variations in the bias magnitudes, with larger biases during the accumulation period (winter and spring) and smaller biases during the ablation period (summer and autumn). The largest bias in winter can be several times larger than the lowest bias in summer. This is because higher seasonal averages of SCF (Fig. S3) may induce larger seasonal bias. Additionally, correlation and STDR (Table S2), and hence SS (Fig. 3, fifth column on left), are better during the accumulation period, indicating that winter and spring have better spatial performance for SCF. MERRA2 and CRAL have the largest seasonal variability in SCF performance (Fig. 3, sixth column on left).

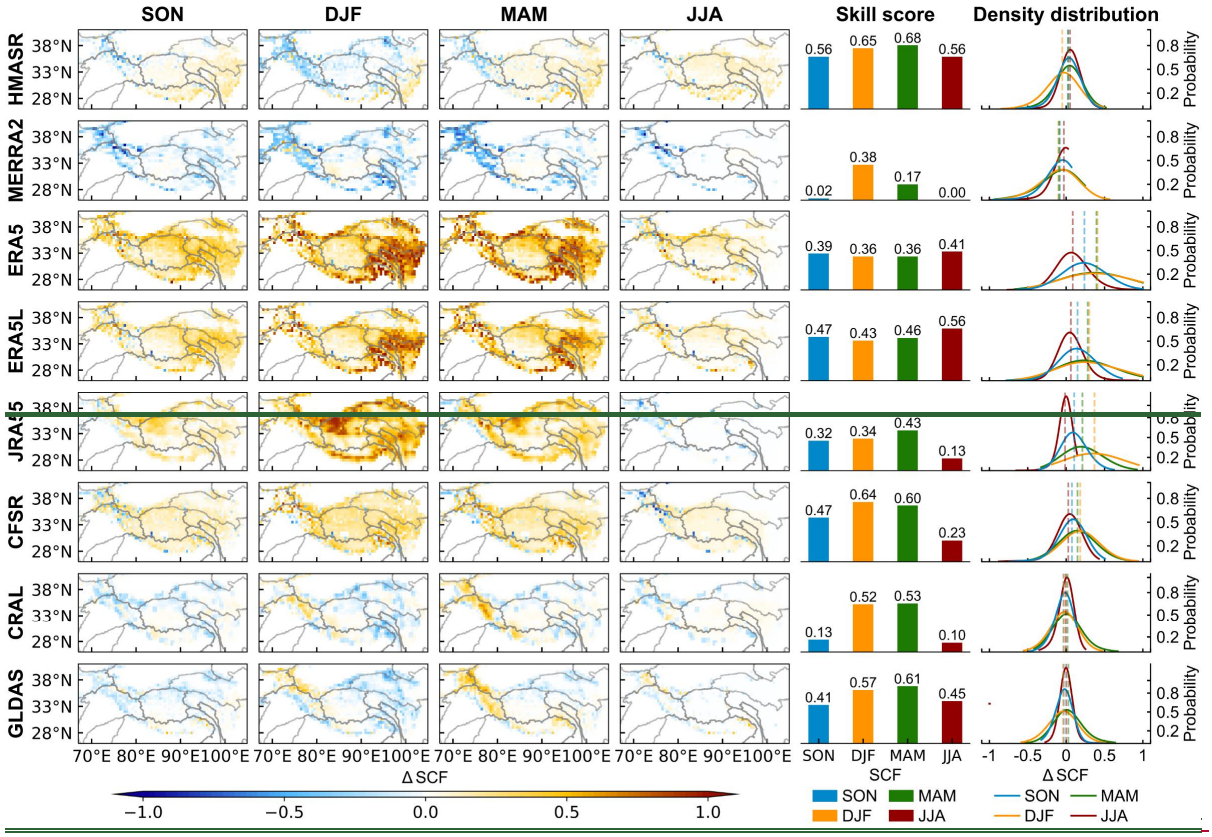

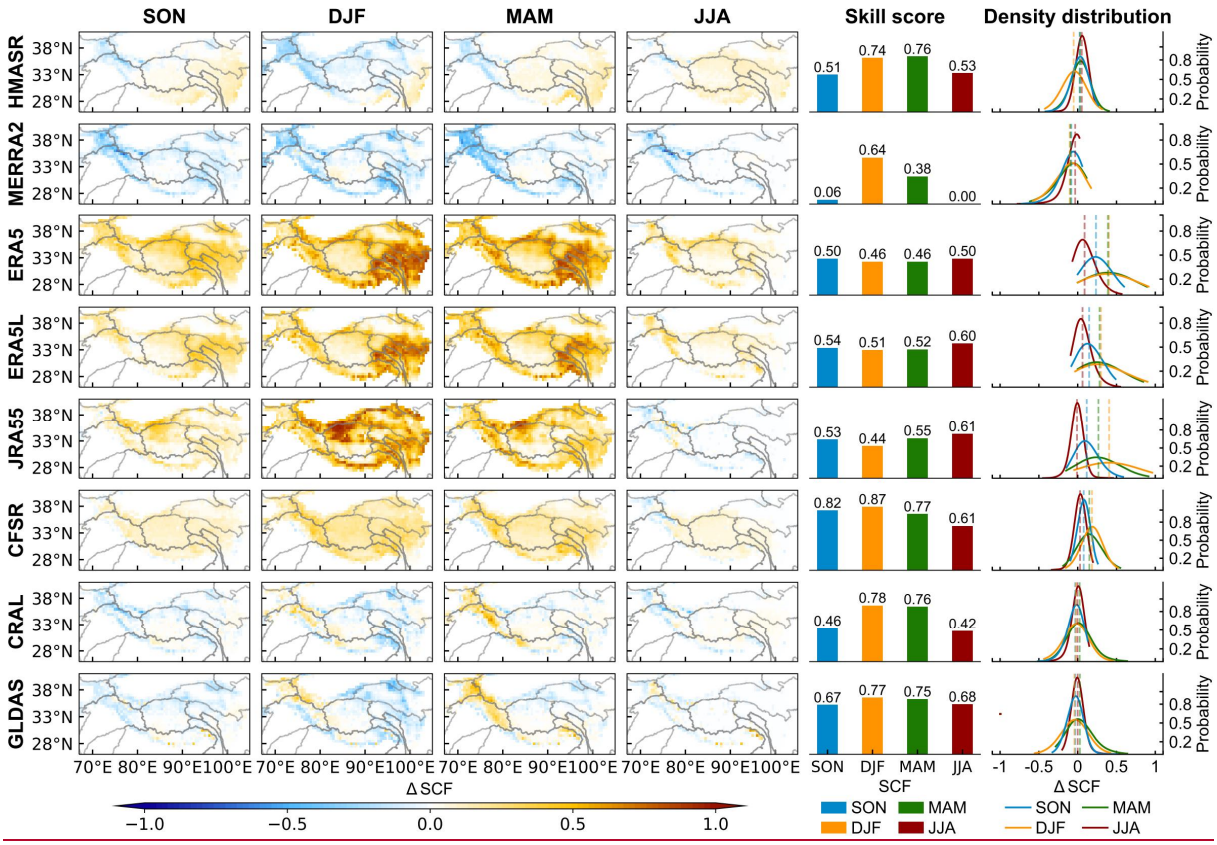

Figure 3: The first four columns show the spatial distribution of seasonal SCF climatological bias from the reanalysis datasets based on SPIReS over the TP during (left to right): autumn (September–November: SON), winter (December–February: DJF), spring (March–May: MAM), and summer (June–August: JJA). The SS values of seasonal SCF climatology are shown in the fifth column. The probability density distribution of seasonal SCF climatological bias is shown in the sixth column. The dashed lines in the sixth column represent the TP-average SCF bias for each season.

3.1.3 Annual variability and trends in SCF

The 17 WY time series of reanalysis datasets has spatially consistent overestimates for ERA5L, ERA5, and JRA55 and an underestimate for MERRA2 (Fig. 4a). Notably, the fluctuations in CFSR around 2010 align with variations in its temperature and snowfall (Fig. S4), likely due to inherent discontinuities in the dataset that cause changes in boundary conditions and subsequently in model output variables (Fujiwara et al., 2017). Additionally, the annual variation of TP-averaged SCF has no significant annual trend in SPIReS (Fig. 4b). ERA5L, JRA55, and GLDAS have annual trends consistent with SPIReS, showing a slight decline and significant correlation, with correlation coefficients above 0.7 (Fig. 4c). Although HMASR and

ERA5 have a slight increasing trend, they remain significantly correlated with SPIReS. Conversely, the correlation of MERRA2, CFSR, and GLDAS with SPIReS did not pass the statistical significance test.

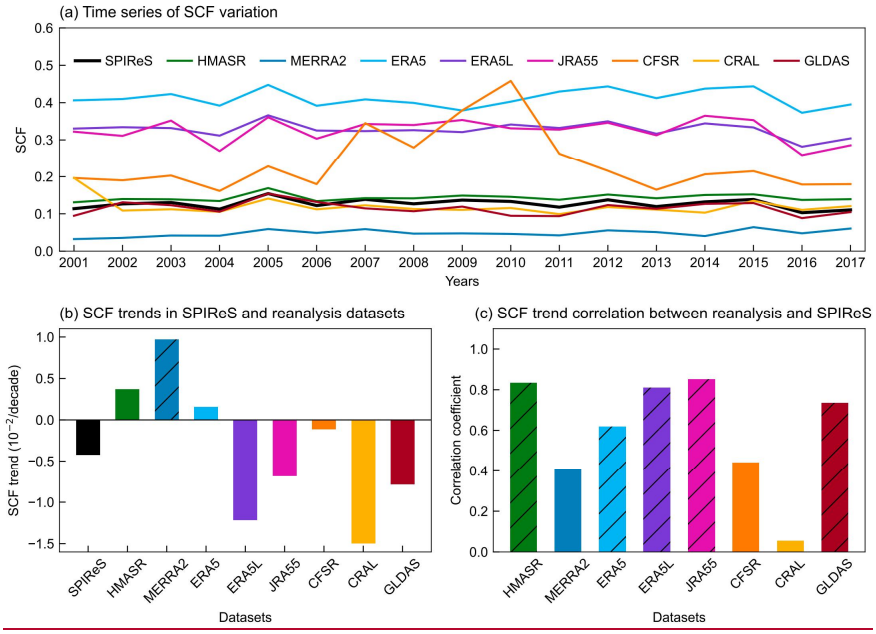

Figure 4: (a) Time series of the annual SCF from SPIReS and eight reanalysis datasets over the TP. (b) The annual trends of SCF from SPIReS and eight reanalysis datasets over the TP. (c) The correlation of SCF annual trends in reanalysis datasets with SPIReS over the TP. Slashes in (b)and (c)indicate that the annual trends and correlation exceeds the 95% confidence level.

We further evaluated the spatial consistency of annual trends in reanalysis datasets with SPIReS (Fig. 5). SPIReS have generally decreased SCF over the westerlies-dominated and the eastern and southeastern monsoon-dominated basins, but increased SCF in the northeastern ITP, the central Brahmaputra, and the northern Yangtze basins. However, these changes are statistically significant in only about 17% of the TP (Fig. 5a). ERA5L, JRA55, and ERA5 have greater variability in SCF annual trends, with significant decreases in the Tarim basin. Nevertheless, they still have relatively high CI values of 0.62, 0.58, and 0.51, respectively (Fig. 5b). This indicates that ERA5L, JRA55, and ERA5 can capture more than half of the SCF annual trend changes over the TP, having the most similar spatial pattern of annual trends compared to SPIReS. In contrast, CFSR has highly uneven SCF annual trends with intermixed increases and decreases across grid cells, resulting in poorer trend performance with a CI value of only 0.39. MERRA2 exhibits significant increasing trends in the Indus basin but fails to

capture the correct decreasing trend in the monsoon-dominated basins. Consequently, it has the lowest CI value of 0.38, with CI values below 0.4 in most basins (Fig. S6). GLDAS has a significant decrease in SCF over more than 60% of the TP, notably differing from SPIReS. Although the widespread significant trends allow GLDAS to capture the most correct significant increase and decrease trends, reaching 16.42% (as indicated by the red and yellow bars in Fig. 5b), it also introduces a major drawback by misjudging too many insignificant SCF fluctuations. Therefore, GLDAS has the lowest CI value, similar to MERRA2. Combination of SCF time series and spatial consistency of SCF annual trend, ERA5L, JRA55, and ERA5 have better temporal performance, while CFSR, MERRA2, and GLDAS perform worse.

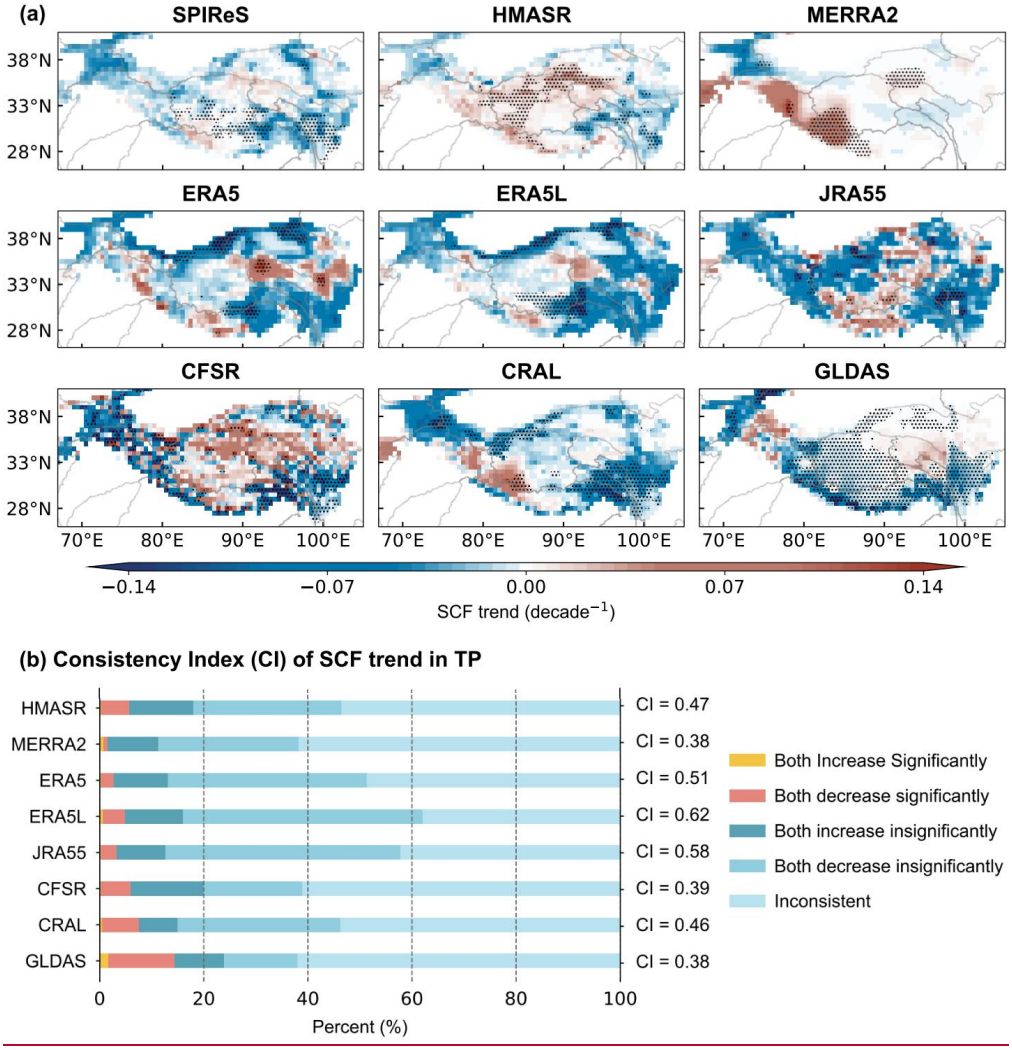

Figure 5: (a) Spatial distribution of the SCF annual trend from SPIReS and eight reanalysis datasets over the TP for the period WY 2001 to WY 2017. (b) The Consistency Index (CI) of SCF trends in reanalysis datasets with SPIReS over the TP.

3.1.2 Bias attribution in the spatial distribution of SCF

3.2.1 Meteorological forcing effects on SCF bias

The evolution of SCF can be determined from the balance between snow mass gain via snowfall and snow depletion via snowmelt, sublimation, and wind drifting (Liu et al., 2022). Both s while snowfall and snowmelt are strongly dependent on temperature (Serquet et al., 2011; Vorkauf et al., 2021). Hence, the accuracy of these two pivotal meteorological forcing factors, snowfall and temperature forcings, directly impacts the accuracy of snow-related variables the integrity of the LSMs (Zhang et al., 2015). In addition, different SCF parameterizations influence the instability inherent in the snow models (Dutra et al., 2011; Jiang et al., 2020), and the data assimilation techniques also affect the final results of SCF simulations (Magnusson et al., 2017). Therefore, wWe further investigated the impact of meteorological factors on SCF bias by examining the performance with respect to snowfall and temperature in each reanalysis dataset, along with the inadequacies of parameterization methods. Moreover, by discussing snow data assimilation among reanalysis datasets, we tried to understand its impact on SCF accuracy.

In the climatological spatial distribution, ERA5, ERA5L, JRA55, and CFSR overestimated snowfall in both both the westerlies-dominated and monsoon-dominated basins, particularly in the Indus and Brahmaputra basins (Fig. 36, first column on left). The snowfall biases are particularly pronounced in the western and southeastern regions of the TP, including on the Pamir Plateau and the southern slopes of Mount Namcha Barwa. The only exception is the inland basin of the ITP, where snowfall is underestimated. ConverselyIn contrast to snowfall, these reanalysis datasets consistently underestimated temperatures in these regions westerlies-dominated and monsoon-dominated basins (Fig. 36, third column on left). Overestimated The excessive snowfall contributes to heightened snow accumulation, while underestimated the reduced temperatures can impede hinder the snowmelt ablation process, leading to an overestimation of snow cover by impeding the snow from attaining the freezing threshold (Liu et al., 2022). Simultaneously, under conditions of adequate atmospheric water vapor, low

~~temperatures further intensify snow accumulation through enhanced snowfall (You et al., 2020b).~~ The combination of overestimated snowfall and underestimated temperatures contributes to the ~~combined impacts result in a~~ positive SCF bias observed in ~~within~~ ERA5, ERA5L, JRA55, and CFSR, evidenced by the significant correlations between snowfall and temperature biases and SCF bias (Fig. 6, second and fourth columns on the left). Additionally, the positive SCF and snowfall biases, as well as negative temperature bias for these reanalysis datasets persist across four seasons, reflecting that the uncertainties in snowfall and temperature data affect the SCF bias year-round (Fig. 7). Compared to snowfall, ~~Furthermore, there are characterized by significant correlations between snowfall and temperature biases versus~~ and ~~SCF bias (Fig. 6, second and fourth columns on the left). Moreover, compared with snowfall, t~~T~~~~t~~emperature bias~~, in particular, exhibits~~ have higher ~~stronger significant~~ correlations with SCF bias and pass significance tests over broader areas (Fig. 6, second and fourth columns on the left). This indicates ~~implies~~ that physical processes influenced by temperature bias may have a more pronounced and widespread responsibility with respect to SCF bias. The temperature biases in ERA5, ERA5L, JRA55, and CFSR also appear to have a greater impact on the seasonal evolution of SCF biases, as evidenced by the higher correlation values (Fig. 7).

For MERRA2, CRAL and GLDAS, the SCF climatology ~~shows~~ has large biases in the westerlies-dominated basins, as well as in the Tarim and Brahmaputra basins (Fig. 2a), where a significant correlation exists between snowfall and temperature biases and SCF bias (Fig. 6, second and fourth columns on the left). This suggests that in these regions, both snowfall and temperature play equally important roles in influencing the SCF biases in MERRA2, CRAL and GLDAS. When considering the TP as a whole, the SCF biases across four seasons for these three datasets align with their well-simulated snowfall (Fig. 7). Therefore, snowfall is likely the primary driver of the seasonal SCF bias.

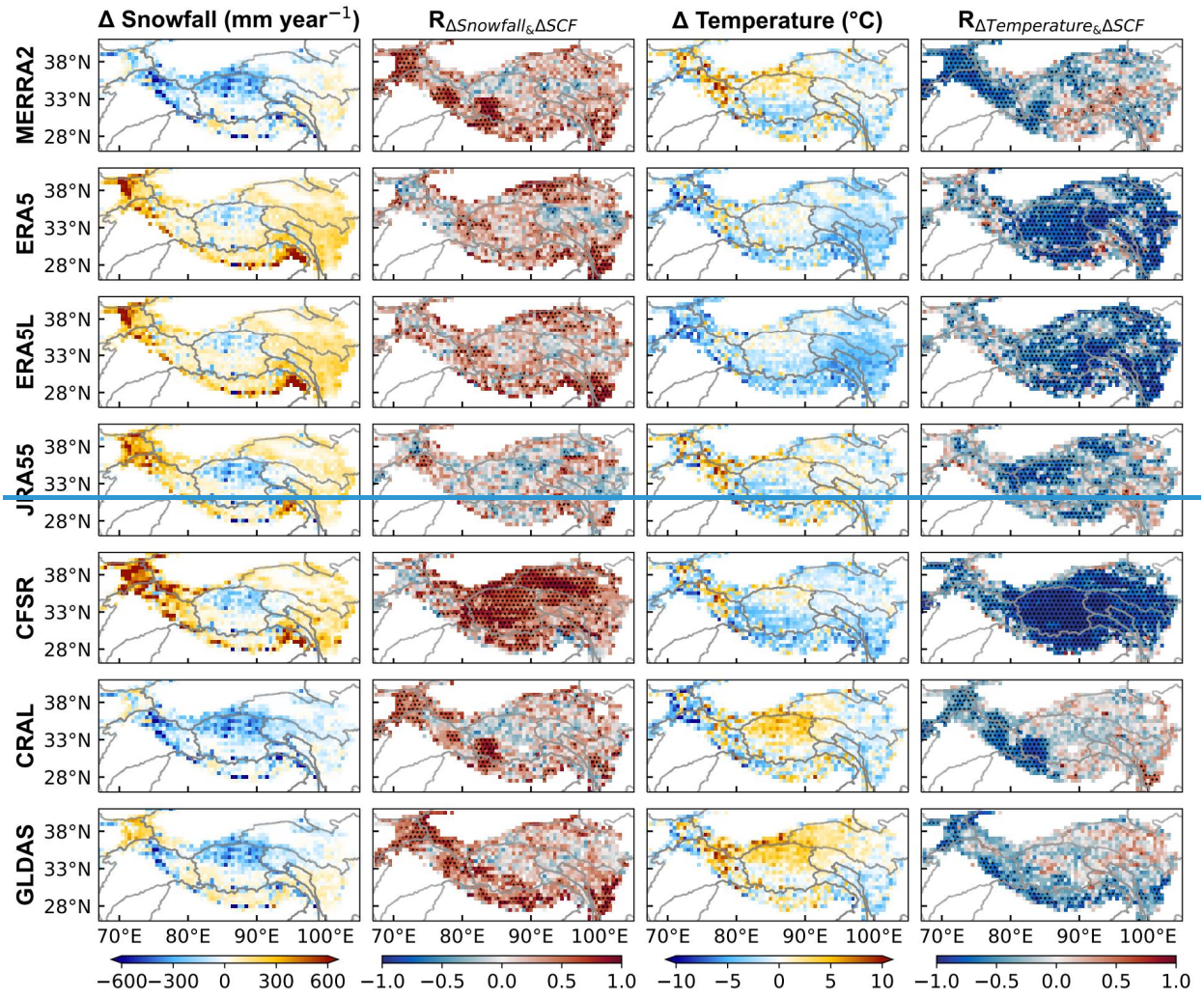
Δ Snowfall (mm year^{-1})
$R_{\Delta Snowfall_{\&}\Delta SCF}$
Δ Temperature (°C)
$R_{\Delta Temperature_{\&}\Delta SCF}$
MERRA2
ERA5
ERA5L
JRA55
CFSR
CRAL
GLDAS
38°N
33°N
28°N
70°E
80°E
90°E
100°E
−600 −300 0 300 600
−1.0 −0.5 0.0 0.5 1.0
−10 −5 0 5 10
−1.0 −0.5 0.0 0.5 1.0

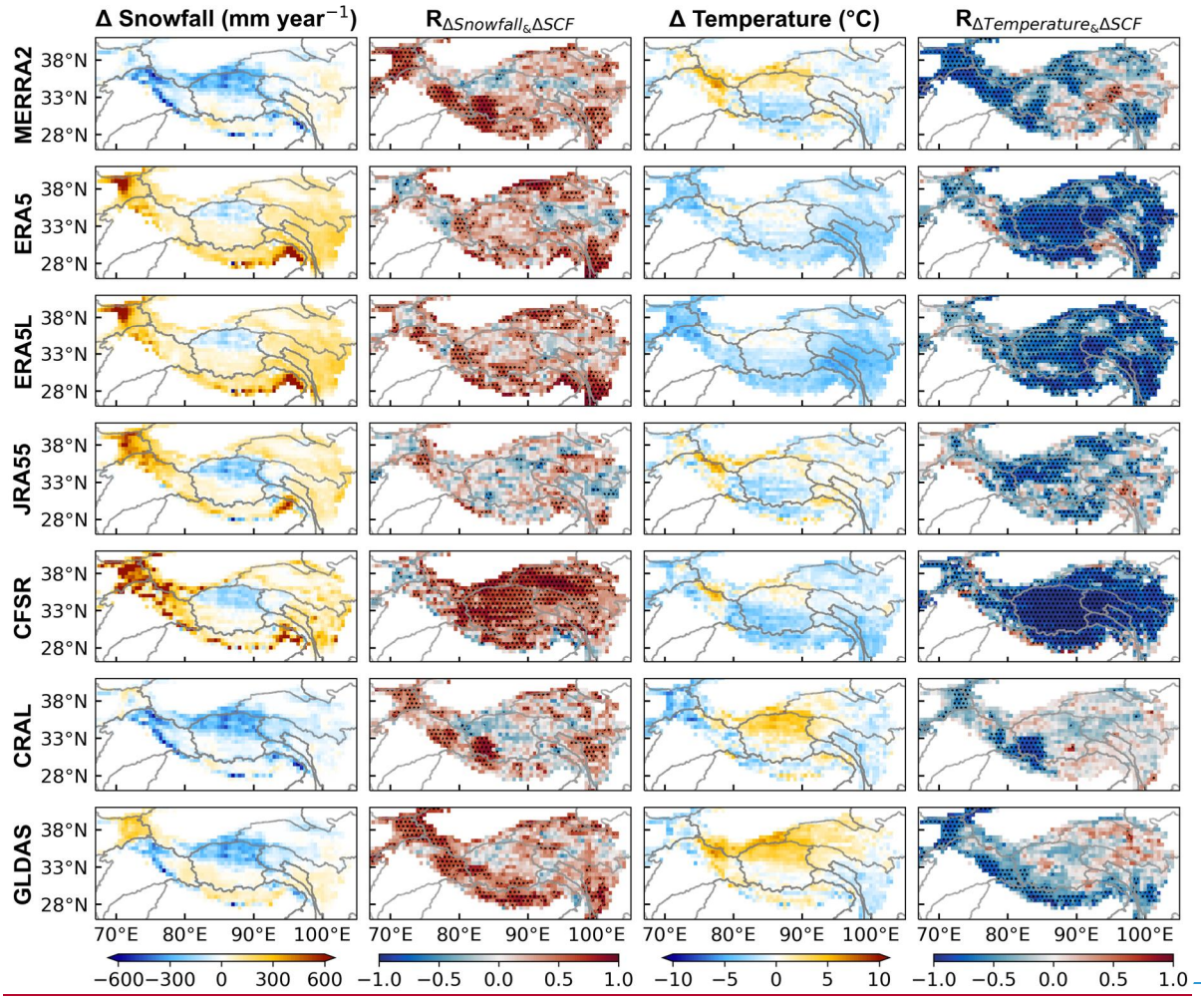

Figure 36: The columns show (from left to right): spatial distribution of the snowfall climatological bias for the reanalysis datasets based on TPMFD over the TP; spatial distribution of the R value between snowfall bias and SCF bias; spatial distribution of the temperature climatological bias for the reanalysis datasets based on TPMFD over the TP; and spatial distribution of R values between temperature bias and SCF bias. Black dots in the second and fourth columns indicate that the correlation exceeds the 95% confidence level. HMASR and MERRA2 share the same meteorological forcing data.

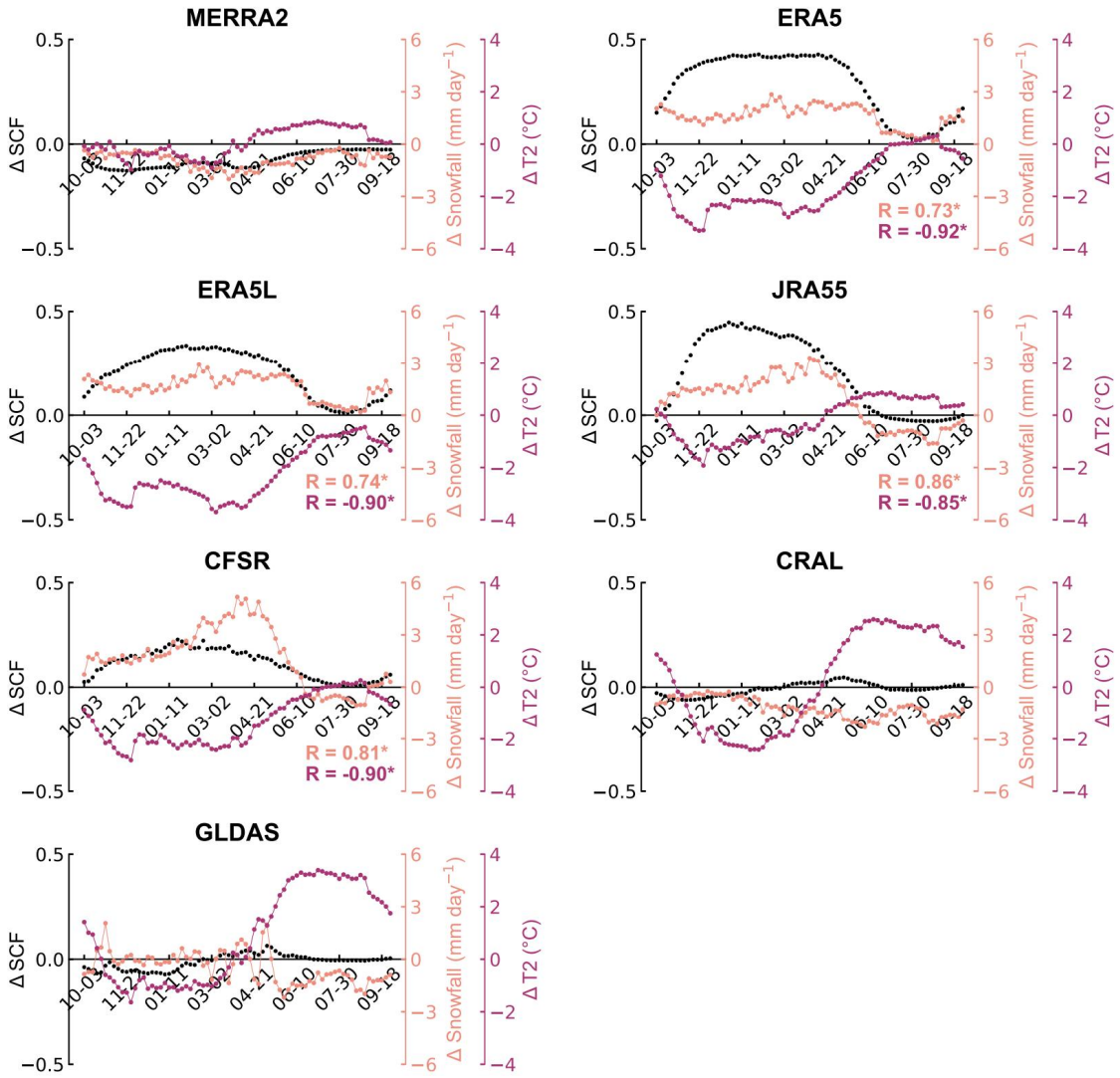

Figure 7: Temporal variations of SCF (black), snowfall (light pink), and temperature (purple) bias averaged at five-day intervals from all reanalysis datasets. R in light pink (purple) represents the correlation coefficient between snowfall (temperature) bias and SCF bias. The stars indicate the correlation exceeds the 95% confidence level. HMASR and MERRA2 share the same meteorological forcing data.

The snowfall and temperature annual trends in most datasets are significantly correlated with their own SCF annual trends (Table S3), indicating that the ability of datasets to capture meteorological factors annual trends influences the simulation of SCF annual trends. ERA5L, JRA55, and ERA5 have correct decreasing snowfall trends and increasing temperature trends in the southeastern monsoon-dominated basins (Fig. 8). Their CI values for meteorological factors trends all exceed 0.5, showing better spatial consistency with TPMFD (Table 2), resulting in better SCF trend simulations. In contrast, MERRA2 has an incorrect significant increase in snowfall over a broad region, except for the Tarim basin (Fig. 8), resulting in a

snowfall CI value of only 0.34 (Table 2) and poorer SCF trend simulations. The highly uneven spatial distribution of annual snowfall and temperature trends in CFSR, as well as the widespread significant trends in GLDAS (with temperature trends significantly increasing in over 90% of the TP), mirror their respective SCF annual trend patterns (Fig. 8). Consequently, CFSR and GLDAS have the lowest CI values for SCF trends (Fig. 5b).

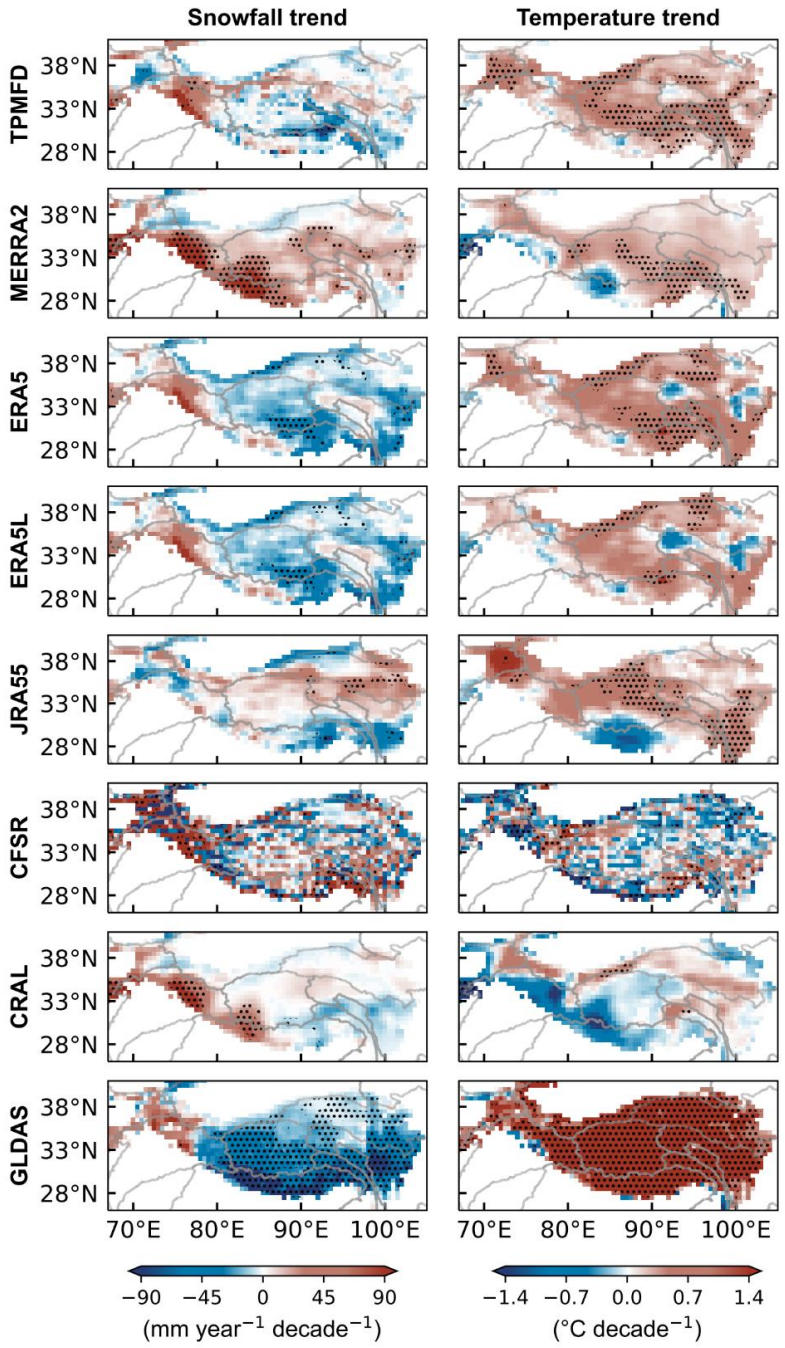

Figure 8: Spatial distribution of the snowfall annual trend from the reanalysis datasets over the TP for the period WY 2001 to WY 2017 (left), and the temperature annual trend (right). Black dots indicate that the trend exceeds the 95% confidence level. HMASR and MERRA2 share the same meteorological forcing data.

Table 2: CI value for snowfall and temperature from eight reanalysis datasets calculated by comparing with TPMFD annual trends from WY 2001 to WY 2017.

	CI values for snowfall	CI values for temperature
MERRA2	0.34	0.58
ERA5	0.54	0.73
ERA5L	0.55	0.59
JRA55	0.54	0.51
CFSR	0.37	0.29
CRAL	0.53	0.30
GLDAS	0.21	0.35

3.2.2 Parameterization approach effects on SCF bias

Different SCF parameterizations influence the instability inherent in the snow models (Dutra et al., 2011; Jiang et al., 2020). We considered the impact of different parameterizations on the spatial distribution and annual trend simulation of SCF for each reanalysis dataset (Fig. 9). ~~JRA55 shows similar patterns and magnitudes of snowfall and temperature biases to ERA5, ERA5L, and CFSR, but these two meteorological factors can explain SCF bias in only limited areas. In addition, Orsolini et al. (2019) found that JRA55 performs well in SD simulation due to assimilating SD data from ground observation stations in China. Thus, the conversion process from SD to SCF within LSM in JRA55 may affect the accuracy of SCF simulations. Indeed, JRA55 uses an aggressive parameterization approach with a 2-cm SD threshold to define the complete SCF, which differs markedly from other reanalysis datasets (see Section 2.1.2 and Table 1). When adopting a more appropriate parameterization method (see Fig. 9), the SCF simulation by JRA55 shows a noteworthy increase in the SS value from 0.37 to 0.5. This apparent improvement confirms the importance of the parameterization method to SCF accuracy in JRA55.~~

~~An interesting observation is that while MERRA2 and HMASR share the same meteorological forcing data but differ in snow assimilation situation. HMASR directly assimilates SCF data obtained from MODIS and Landsat satellites (Liu et al., 2021), which are processed using a spectral unmixing algorithm that has been found more accurate than the original band ratio~~

methods (Stillinger et al., 2023). Therefore, the assimilation of high-precision satellite SCF data enhances the SCF simulation in HMASR, while the lowest SS value obtained by MERRA2 in SCF spatial simulations was likely related to its lack of SCF data assimilation. As for JRA55 and CFSR, which although assimilated SD data and have been found good simulations in SD and SWE (Bian et al., 2019; Orsolini et al., 2019), the process of transforming SD to SCF through model parameterization introduced additional errors, thereby leading SD assimilation to only a limited effect on the accuracy of SCF simulations. Compared to JRA55, the SCF parameterization method employed in CFSR is more reasonable, resulting in spatial simulation performance batter than JRA55 by a considerable margin. This indirectly illustrates the impact of parameterization methods on the SCF simulation in JRA55.

3.2 Seasonal evolution and annual trends in SCF

3.2.1 Evaluation of seasonal evolution and bias attribution

Figure 4 shows the SCF bias, its probability density distribution, and the SS values for the four seasons. In general, the different seasons show similar spatial patterns of SCF bias for each reanalysis dataset, which is consistent with the climatological SCF bias results (Fig. 2a). This suggests the persistent influence of the uncertainties associated with the snowfall and temperature data, on the SCF bias throughout the year. However, the bias values vary seasonally (Fig. 4), with higher biases observed during the accumulation period (winter and spring), but lower biases during the ablation period (summer and autumn). The largest bias in winter can be several times larger than the lowest bias in summer. However, this does not imply a better SCF simulation for summer than winter. As the SCF during winter is much higher than that during summer (Fig. S3), a smaller fractional difference in winter can result in a larger absolute bias. Conversely, higher R values and better STDR values (in other words, STDR closer to 1) in seasonal SCF between the reanalysis datasets and SPIReS are obtained during the accumulation period than the ablation period (Table S2), leading to a better SCF spatial performance for winter and spring, as shown by the larger SS values (Fig. 4). The seasonal variability associated with the SCF simulation performance is most evident in MERRA2 and CRAL.

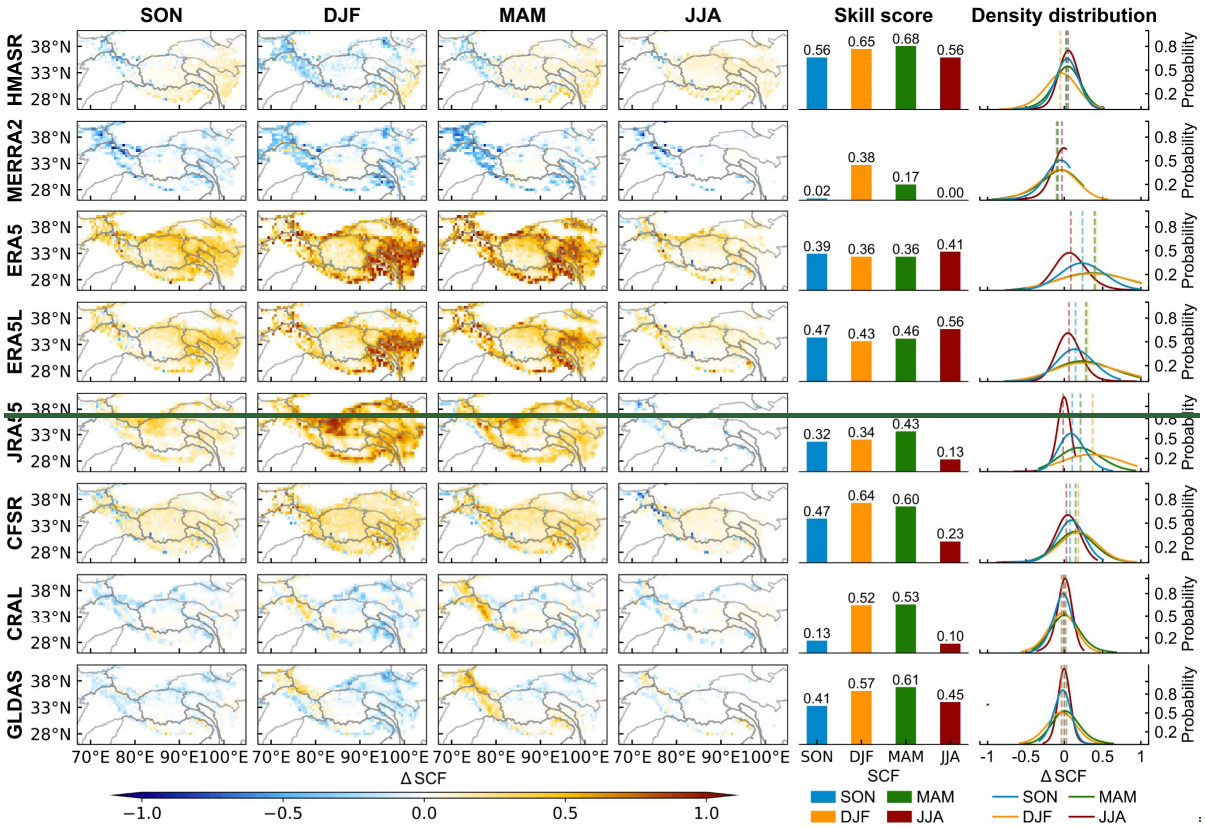

Figure 4: The first four columns show the spatial distribution of seasonal SCF climatological bias from the reanalysis datasets based on SPIReS over the TP during (left to right): autumn (September–November: SON), winter (December–February: DJF), spring (March–May: MAM), and summer (June–August: JJA). The SS values of seasonal SCF climatology are shown in the fifth column. The probability density distribution of seasonal SCF climatological bias is shown in the sixth column. The dashed lines in the sixth column represent the TP-average SCF bias for each season.

Figure 5 further shows the seasonal evolution of the SCF bias, as well as the snowfall and temperature biases. For the four reanalysis datasets, including ERA5, ERA5L, JRA55, and CFSR, snowfall (temperature) shows large positive (negative) biases during the accumulation period, which together cause the large positive SCF bias during winter and spring. In contrast, both the snowfall and temperature biases are small during the ablation period, resulting in a small SCF bias. Thus, snowfall and temperature collectively explain the apparent seasonal variations in the SCF bias, as evidenced by the statistically significant correlations. Compared with snowfall, the temperature bias seems to have a greater impact, which is characterized by the larger R values. For MERRA2, CRAL, and GLDAS, the SCF biases remain small and stable

~~across all four seasons, which corresponds to the well simulated snowfall, despite the highly variable temperature bias. Therefore, snowfall may be more responsible for the seasonality in the SCF bias associated with these three reanalysis datasets.~~

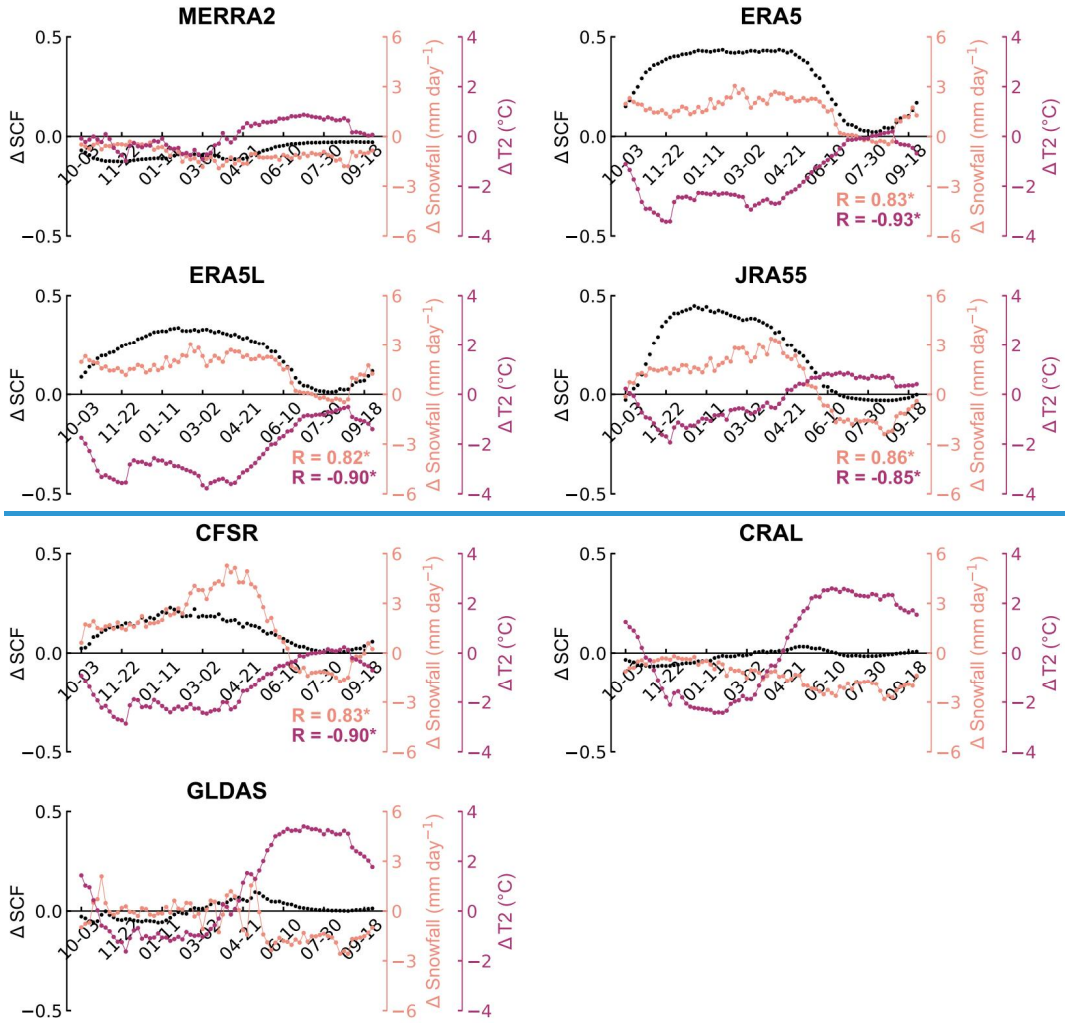

~~Figure 5: Temporal variations of SCF (black), snowfall (light pink), and temperature (purple) bias averaged at five-day intervals from all reanalysis datasets. R in light pink (purple) represents the correlation coefficient between snowfall (temperature) bias and SCF bias. The stars indicate the correlation exceeds the 95% confidence level. HMASR and MERRA2 share the same meteorological forcing data.~~

~~3.2.2 Evaluation of annual trends and bias attribution~~

~~Figure 6 presents the annual trends in SCF from WY 2001 to WY 2017 for the SPIReS and eight reanalysis datasets, as well as the CI values that characterize the agreement in SCF annual trends between the reanalysis datasets and SPIReS. The SPIReS generally show decreased SCF~~

~~over the westerlies-dominated and east and southeast monsoon-dominated basins, but increased SCF over the east ITP, central Brahmaputra, and north Yangtze basins. However, these trends are not statistically significant over most areas of the TP, indicating fluctuations in the variability of SCF over the past 17 years. This insignificant distribution over a wide area is also clearly demonstrated by snowfall trends in TPMFD (Fig. 7).~~

~~In comparison to SPIReS, ERA5L, ERA5, and JRA55 show greater variability in SCF annual trends, particularly noticeable in the Tarim basin and southeastern TP, where a significant decrease in SCF is evident (Fig. 6a). Nevertheless, ERA5L, ERA5, and JRA55 still exhibit the most similar spatial patterns to SPIReS, with relatively high CI values for SCF trends in the TP, specifically 0.51, 0.48, and 0.49 respectively (Fig. 6b). This indicates their relatively well annual trends performance among the eight reanalysis datasets and can reproduce the SCF annual trend approximately half of the TP. This can be attributed to the superior spatial consistency of ERA5L, ERA5, and JRA55 in simulating snowfall and temperature annual trends when compared with TPMFD (Fig. 7), as evidenced by CI values exceeding 0.5 for both snowfall and temperature annual trends (Table S3). For JRA55, suboptimal parameterization methods primarily affect the numerical magnitude of SCF simulation, resulting in higher RMSE and lower SS values in SCF climatological spatial distribution (see Section 3.1). However, the parameterization process has minimal impact on the fluctuating variations of SCF over the time series, allowing JRA55 to demonstrate good annual trend performance (Fig. 6).~~

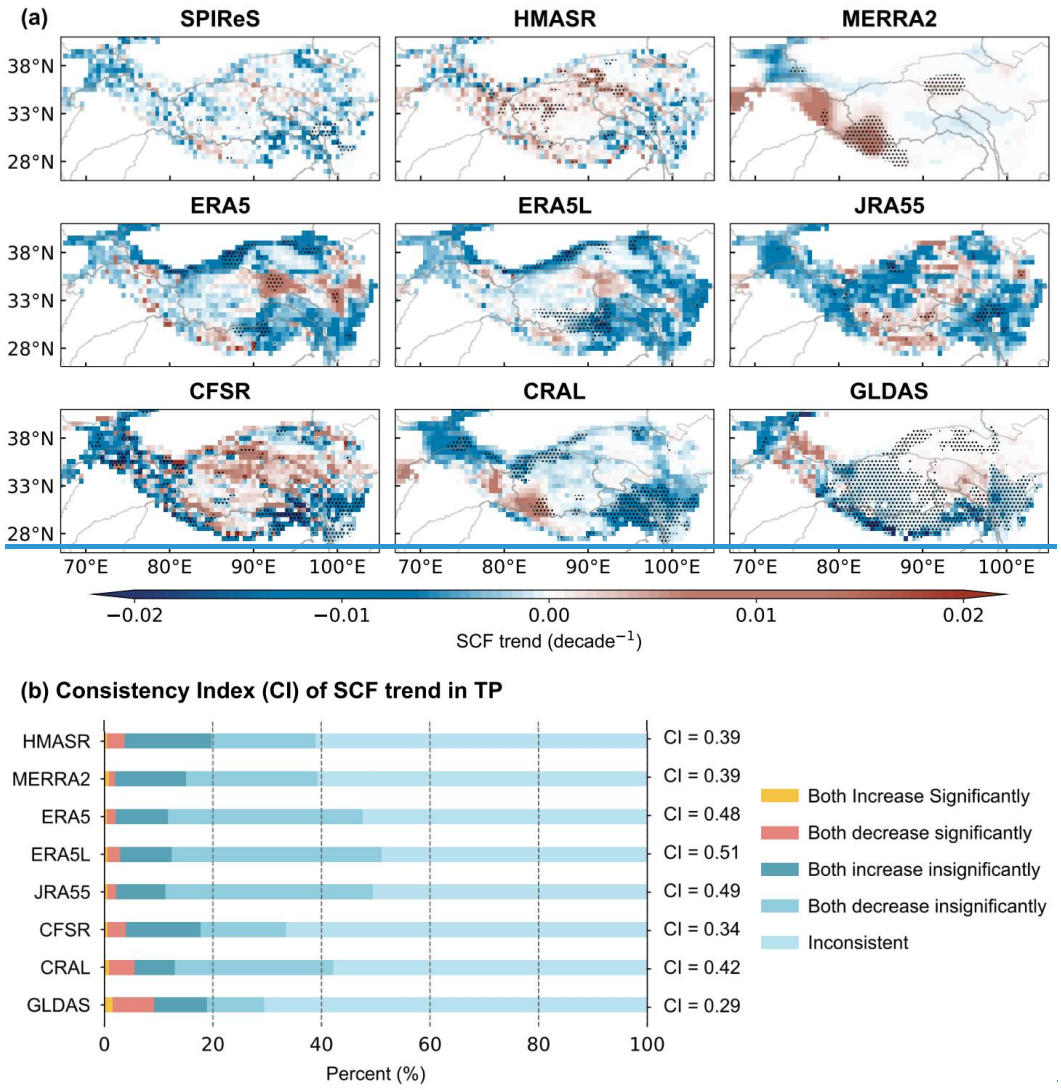

~~Figure 6: (a) Spatial distribution of the SCF annual trend from SPIReS and eight reanalysis datasets over the TP for the period WY 2001 to WY 2017. (b) The Consistency Index (CI) of SCF trends in reanalysis datasets with SPIReS over the TP.~~

~~The SCF annual trend of CRAL is statistically significant over approximately half of the TP, different from SPIReS. Consequently, CRAL demonstrates moderate performance in simulating SCF annual trends, similar to its spatial performance. CFSR presents highly uneven SCF annual trends with intermixed increases and decreases across pixel points, mirroring its snowfall and temperature annual trend distributions, resulting in poorer SCF annual trend performance with a CI value of only 0.34. GLDAS shows a significant decrease in SCF over more than 75% of the TP, markedly differing from SPIReS. While the widespread significant trends allow GLDAS to capture the most correct trends, reaching 9.25% (as indicated by the red and yellow bars in Fig. 6b), it also introduces a major drawback by misjudging too many insignificant SCF~~

fluctuations. Therefore, GLDAS has the lowest CI value of 0.29, with most basins having a CI value below 0.3 (Fig. S4). This is associated with its widespread and significant decreases in snowfall and increases in temperature annual trends (Fig. 7).

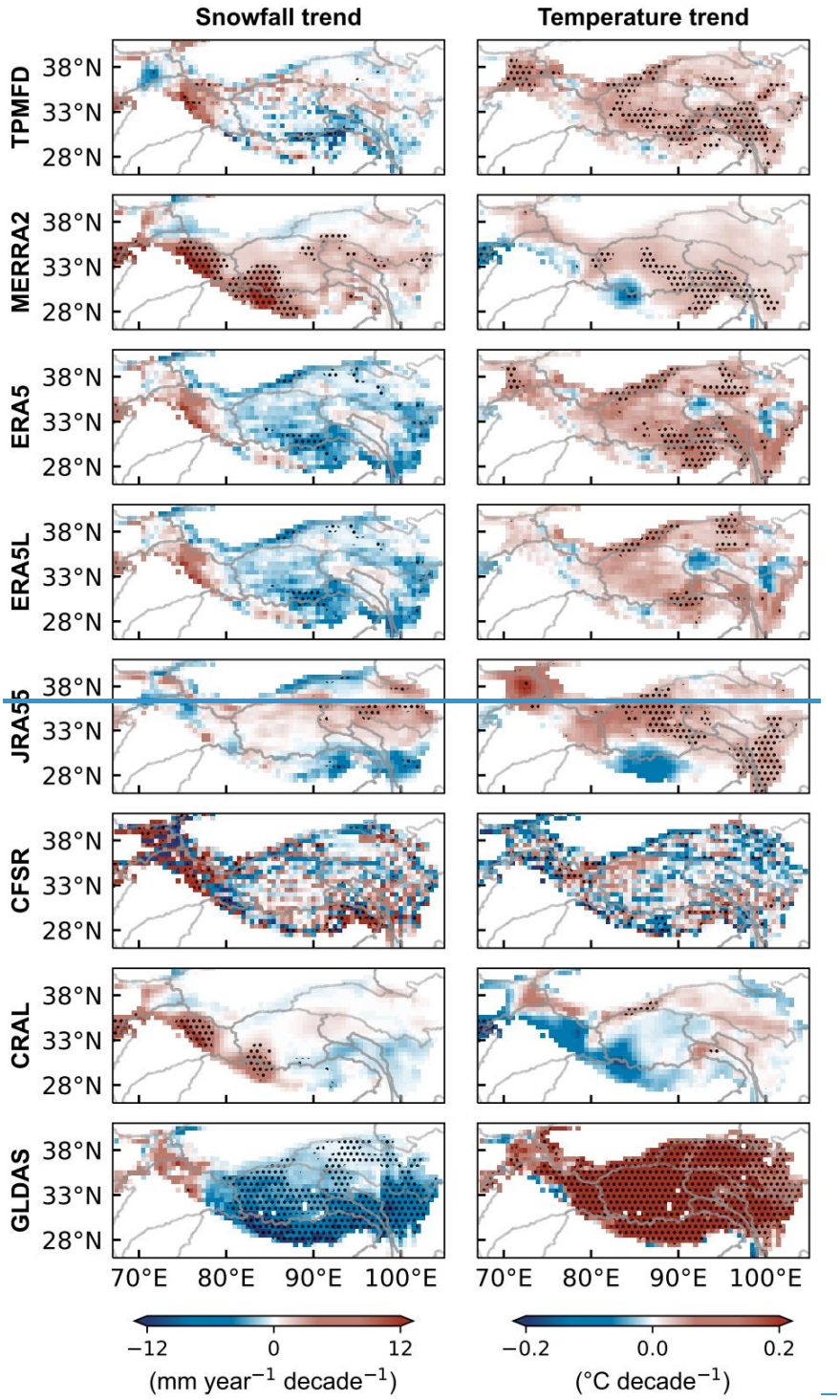

Figure 8: Spatial distribution of the snowfall annual trend from the reanalysis datasets over the TP for the period WY 2001 to WY 2017 (left), and the temperature annual trend (right). Black dots indicate that the trend exceeds the 95% confidence level. HMASR and MERRA2 share the

same meteorological forcing data.

MERRA2 depicted a significantly increase trend in the southwestern TP, not align with SPIReS. This discrepancy is linked to MERRA2's erroneous portrayal of a significant increase in snowfall and a significant decrease in temperature in this region (Fig. 7). In contrast, HMASR, forced by the same meteorological input fields as MERRA2, partly corrected the falsely increase SCF trend in the southwestern TP and succeeded in capturing a significant declining trend in the southeastern TP, compared to MERRA2. This is evidenced by a higher proportion of correct significant trends (indicated by the red and yellow bars in Fig. 6b being greater for HMASR than for MERRA2). Moreover, the spatial pattern of HMASR SCF annual trends is more similar to SPIReS than MERRA2. However, when considering TP as a whole, the SCF trend simulations by HMASR showed limited improvement compared to MERRA2 as indicated by the similar CI values, yet still underperformed compared to ERA5L, ERA5, and JRA55. This suggests that data assimilation can only partially enhance SCF trend simulations, with meteorological forcings remaining the primary influencing factors.

4 Discussion

4.1 Influence of parameterization method on SCF

Figure 9 shows the SS and CI values of SCF simulations from each reanalysis dataset using the different parameterization methods. TheThe parameterization process primarily affects the SCF values, while its impact on the phase of fluctuations in SCF time series is limited, as evidenced by the small variations in CI values among the reanalysis datasets (Fig. 9b). value rather than the SCF phase variation over the time series, Therefore, so the our focus is on the on the spatial performance of the parameterization-improved SCF simulation, spatial performance induced by the different parameterizations reflecting among the reanalysis datasets, indicated by the spatial distribution of SCF bias (Fig. S7) and SS values (Fig. 9a) obtained.

For most reanalysis datasets, tThe MM_SCF method improves generates the best SCF spatial simulation in ERA5, ERA5L, JRA55, HMASR, and CFSR, reducing biases and increasing SS values, in terms of spatial performance with higher SS among most reanalysis datasets. This advantage is especially distinct for MERRA2 and ERA5. Moreover MM_SCF

~~performs better than the built-in methods in ERA5, ERA5L, CRAL, and JRA55, demonstrating~~ demonstrating its ~~its~~ broad applicability. Meanwhile, the MM_SCF method is applicable in most of the basins (Fig. S8). The ~~performance of~~ ME_SCF method ~~is~~ also slightly enhances the spatial performance of some dataset (Fig. 9a)~~good, with SS values slightly lower than those of MM_SCF~~. The Noah_SCF method, which accounts for the complex influence of underlying surface characteristics on SCF, has spatial performance comparable to MM_SCF and ME_SCF. This indicates that surface characteristics have a limited impact on spatial SCF accuracy. In contrast to the parameterization above, the aggressive MJ_SCF approach with a 2-cm SD threshold to define the complete SCF (Table 1), reduces the spatial performance of all datasets, particularly in JRA55~~ generally results in the poorest spatial performance across most reanalysis datasets, including JRA55~~, which uses MJ_SCF as its built-in method. Additionally, SCF obtained using the MJ_SCF method for all reanalysis datasets have large positive biases (Fig~~ure~~. S~~XXX~~7), further reflecting its inapplicability. Orsolini et al. (2019) found that JRA55 performs well in SD simulation due to assimilating SD data from Chinese ground observation stations. When adopting a more appropriate method to transform SD into SCF, the bias of JRA55 significantly decreased, and the SS value increases from 0.57 to 0.81, comparable to the best-performing CFSR (Fig. 9a). This apparent improvement confirms the importance of parameterization to JRA55 SCF accuracy. Apart from JRA55, optimizing ~~For the Noah_SCF methods, although they incorporate the complex impacts of the underlying surface characteristics on SCF parameterization, the spatial performance of SCF is only comparable with that of MM_SCF and ME_SCF. This implies that considering the underlying surface characteristics has a limited impact on the accuracy of the SCF spatial simulations. We note that~~ parameterization ~~an appropriate parameterization method can actually improve SCF simulation. However, such improvements~~ does not significantly alter the spatial performance ranking of the eight reanalysis datasets~~; . for~~ For example,~~instance,~~ the SS values for MERRA2, ERA5, and ERA5L~~, and JRA55~~ using the optimal MM_SCF method are still lower than those for ~~HMASR~~ CFSR using the poorest MJ_SCF method. This indirectly highlights the primary role of

snowfall and temperature ~~meteorological~~ forcing inputs ~~(snowfall and temperature) and snow assimilation~~ with respect to SCF simulations.

~~The influence of parameterization methods on the temporal performance of the datasets, excluding CRAL, is limited, as indicated by small variations in the CI values among the reanalysis datasets.~~

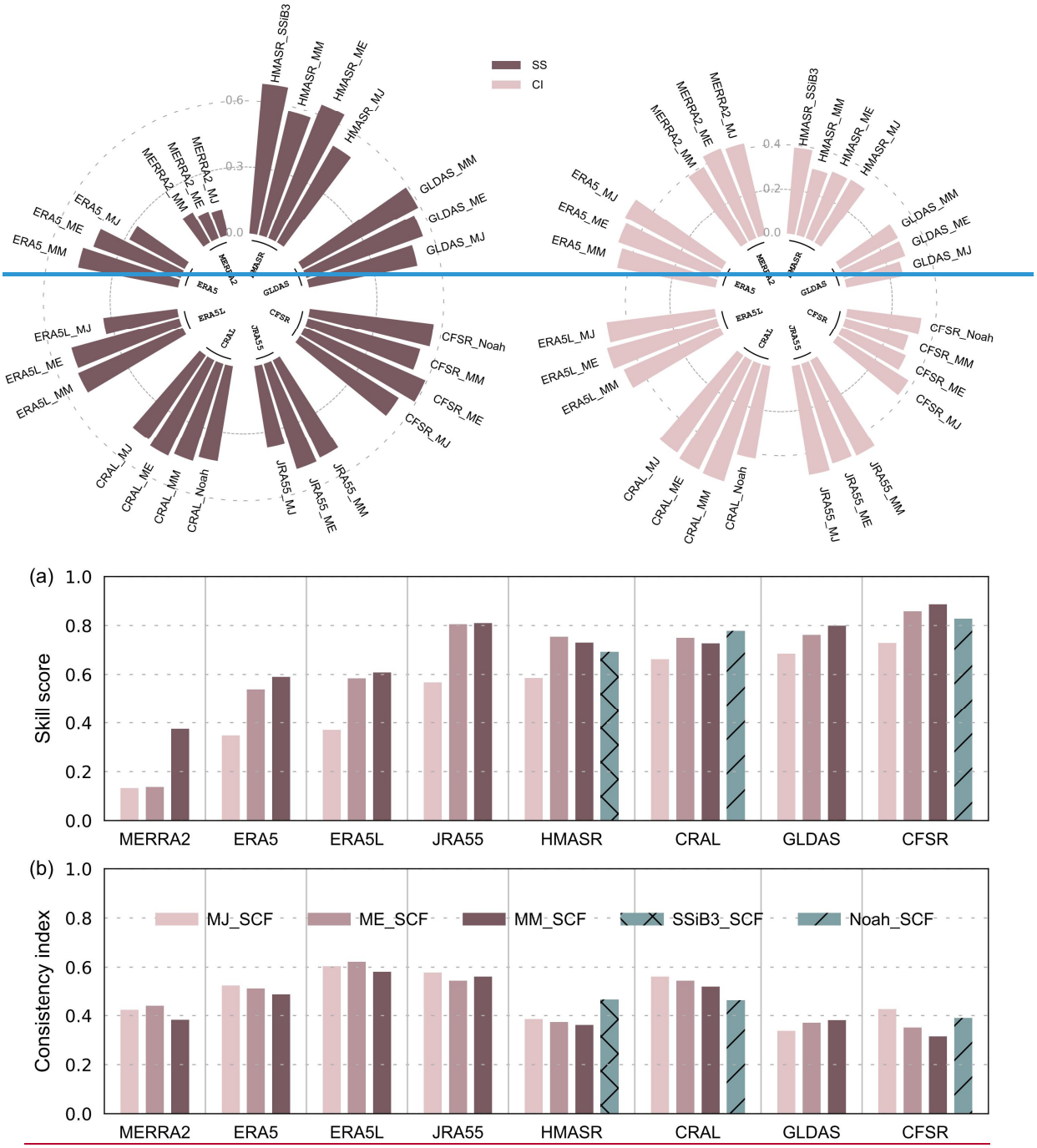

Figure 9: SS (~~left~~a) and CI (~~right~~b) values of SCF for all reanalysis datasets calculated offline using the MM_SCF, MJ_SCF, and ME_SCF parameterization methods. The green bars represent the built-in parameterization methods for HMASR, CRAL, and CFSR.

4.23.3 Combination of Reanalysis reanalysis dataset ensemble for SCF optimization

To optimize SCF simulation over the TP, we considered all possible combinations of the eight reanalysis datasets, identifying the best and worst combinations regarding both the spatial distribution and annual trend (Fig. 10). Combining datasets can improve SCF accuracy, as evidenced by the SS and CI values of all combined datasets being higher than those of the single best-performing dataset (Fig. 10). However, Our results reveal that the SCF accuracy does not monotonically improve with the number of combined datasets. For the sSpatially aspect, the SS value improves when transitioning from CFSR HMASR alone to a combination with GLDAS and HMASRGLDAS, but declines when more datasets are combined (Fig. 10a). The SS value with four datasets combined is lower than that achieved with HMASR alone, indicating that merging additional datasets does not always improve simulation accuracy, and may instead have a negative impact. Consequently, we concluded that a combination of HMASR and GLDAS is optimal for spatial SCF studies over the TP. This appears reasonable because CFSR, GLDAS, and HMASR HMASR and GLDAS have excellent accuracy in simulating SCF the spatial variability of SCF, but adding the addition of poorly performing datasets (e.g., MERRA2 and JRA55) introduces more bias, resulting in a suboptimal outcome. Consequently, we concluded that a combination of CFSR, GLDAS, and HMASR is optimal for spatial SCF studies over the TP. TemporallyFrom the trend aspect, the highest CI values are is achieved with by the combination of more the three best-performing datasets for SCF annual trends, namely ERA5L, JRA55, HMASR, ERA5, GLDAS, and CRALERA5L, JRA55, and ERA5, which is different from the SS results (Fig. 10b). Unlike SS, combining more datasets does not lead to a rapid decrease in CI values. The CI value from combining seven datasets still surpasses that obtained from ERA5L alone. This is because reanalysis datasets generally Given the minor annual trend changes in SCF over the 17 years, all reanalysis datasets struggle to capture significant trend variations, displaying have moderate SCF annual trend performance. C. Thus, eombining more datasets can helps mitigate the shortcomings of individual datasets and improve the, enhancing overall annual trend accuracy. In contrast to the optimal combination, the worst combination shows a monotonically and significantly improving performance for

both spatial distribution and annual trends with increased number of combined datasets (Fig. 10c and 10d). ~~Notably, the worst combinations for SS and CI consistently include MERRA2 and GLDAS, whereas HMASR and ERA5L consistently contribute to the optimal combination for SS and CI. This corresponds with the results in Section 3.~~

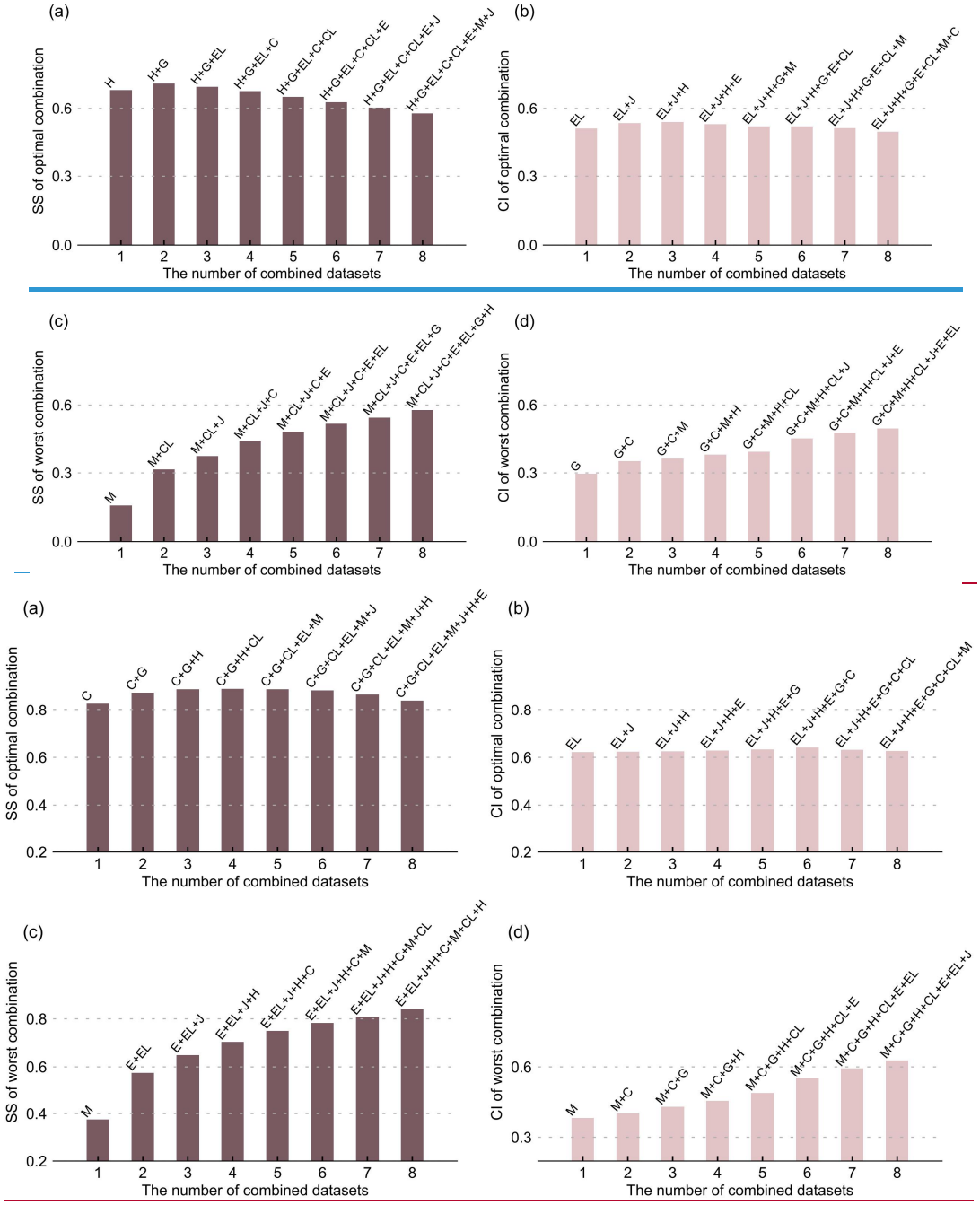

Figure 10: (a) SS for optimal reanalysis dataset combinations across varying numbers of datasets. (b) As in (a) but for CI. (c) and (d) As in (a) and (b), but for the worst combinations. H: HMASR; M: MERRA2; E: ERA5; EL: ERA5L; J: JRA55; C: CFSR; CL: CRAL; G: GLDAS.

4 Discussion

4.1 Effects of data assimilation, resolution, and LSMs

Data assimilation is an effective approach for reducing snow model uncertainties and enhancing the capability to monitor seasonal snow changes (Andreadis and Lettenmaier, 2006; Sun et al., 2004). HMASR directly assimilates SCF data obtained from MODIS and Landsat satellites (Liu et al., 2021), which are processed using a spectral unmixing algorithm that has been found more accurate than the original band ratio methods (Stillinger et al., 2023). Under the same meteorological input fields as MERRA2, the data assimilation in HMASR corrects the widespread SCF underestimation and erroneous trends in the southwestern TP exhibited by MERRA2, enhancing the spatiotemporal simulation performance of HMASR. ~~However~~In contrast, lowest SS and CI values in SCF spatiotemporal simulations for MERRA2 ~~are~~may be ~~likely~~ partly related to its lack of SCF data assimilation. JRA55 and CFSR assimilate SD data and show good simulation performance in SD and SWE (Bian et al., 2019; Orsolini et al., 2019). However, the process of converting SD to SCF in JRA55 introduces additional errors, limiting the impact of SD assimilation on SCF spatial simulation accuracy. In contrast, CFSR employs a more reasonable SCF parameterization, resulting in significantly higher spatial simulation performance compared to JRA55. This indirectly highlights the influence of parameterization methods on SCF simulation in JRA55.

The spatial resolution of reanalysis datasets and the choice of LSM may also affect the accuracy of SCF simulations. Lei et al. (2023) pointed out that reanalysis datasets characterized by finer spatial resolutions exhibit better consistency with in situ measurements of SD over the TP; e.g., ERA5L outperforms ERA5 and MERRA2. Sun et al. (2023) evaluated the ability of different LSMs to simulate SD in China based on station observation data and found that the community Noah LSM with multi-parameterization options (Noah-MP model) provided the best overall performance. In our study, the fine spatial resolution version of GLDAS generates better SCF simulations than the coarse spatial resolution version for both spatial distribution and annual trend (Fig. S1). Additionally, compared to the CLSM and VIC models, GLDAS

simulations using the Noah model show better SCF performance at a 1°×1° resolution. This indicates the non-negligible impact of model resolution and LSM choice on SCF simulation accuracy. However, SCF products with different spatial resolutions and LSMs are available only in GLDAS. Therefore, this study cannot conclusively state that the impact of spatial resolution and LSM on SCF accuracy is universal.

4.2~~3~~ Limitations

This study focused primarily on the impact of snowfall and temperature factors ~~with~~in snow models, as well as ~~snow data assimilation and~~ the choice of SCF parameterization, on the performance of reanalysis datasets in simulating SCF over the TP. However, other model parameters related to precipitation and temperature, such as the precipitation gradient used to describe precipitation variations at different elevations, and the critical temperature used to distinguish rain from snow, are equally vital to snow simulations (Zhang et al., 2015). Furthermore, snow, being a suspended substance, is susceptible to sublimation. It is estimated that blowing snow sublimation accounts for ~30% of global surface sublimation (Déry and Yau, 2002). The TP is perpetually influenced by the westerly jet stream, and processes such as blowing snow sublimation may be significant under windy and arid conditions. However, most LSMs used in reanalysis datasets do not consider blowing snow (Mortimer et al., 2020), and deficiencies in their model structures may also affect the accuracy of SCF simulations.

~~In addition to these factors, the spatial resolution of reanalysis datasets and may also affect the accuracy of SCF simulations. Lei et al. (2023) pointed out that reanalysis datasets characterized by finer spatial resolutions exhibit better consistency with in situ measurements of SD over the TP; e.g., ERA5L outperforms ERA5 and MERRA2. In our study, the fine spatial resolution version of GLDAS generates better SCF simulations than the coarse spatial resolution version for both spatial distribution and annual trend (Fig. S1), which demonstrates the non-negligible impact of model resolution on the accuracy of SCF simulations. This also indirectly implies that the much finer resolution of 1/225° × 1/225° may contribute to the outstanding performance of HMASR. However, SCF products with different spatial resolutions~~

~~are available only in GLDAS. Therefore, this study cannot conclusively state that the impact of spatial resolution on SCF accuracy is universal.~~

5. Conclusions

~~Snow cover on the TP is sensitive to climate change. With global climate warming, the quantity and variability of SCF have become crucial indicators for understanding climate change and related hydrological processes. In t~~This study evaluates~~, we assessed~~ the ability and attributed the biases of eight widely used reanalysis datasets to simulate spatiotemporal variations in SCF over the TP based on SPIReS ~~data~~ covering the period WYs 2001–2017. The results indicate that CRAL, GLDAS, and HMASR agree best with SPIReS in TP-averaged SCF and SS values all exceeding 0.7. CFSR, despite overestimating SCF, has the highest SS value due to good correlation with SPIReS and a high STDR value. These four datasets perform well spatially. In contrast, ERA5, ERA5L, and JRA55 generally overestimate SCF, while MERRA2 consistently underestimates it, leading to poor spatial performance. Overall, the reanalysis datasets exhibit moderate accuracy in annual trend analysis. ERA5L, JRA55, and ERA5 have relatively good temporal performance, with significant correlation in trend time series and better CI values in trend spatial consistency. GLDAS and CFSR perform poorly in trend representation. While MERRA2 has the worst performance in both spatial distribution and annual trend.

Snowfall and temperature significantly impact SCF bias. ERA5, ERA5L, and JRA55 overestimate SCF due to overestimated snowfall and underestimated temperature. Temperature-related physical processes have a more significant impact on SCF bias and its seasonal variations in these datasets. The poor trend performance in GLDAS and CFSR is due to inconsistent between temperature and snowfall trends compared to TPMFD trends. Meteorological factor errors impact the poor spatiotemporal performance of MERRA2. Additionally, the overestimation of SCF in JRA55 is also linked to aggressive parameterization. Except for JRA55, parameterization optimization improves SCF but does not significantly alter the spatial performance ranking of the eight reanalysis datasets. To improve SCF accuracy, combining datasets is an effective method. ~~The key findings are:~~

~~Among the eight reanalysis datasets, HMASR shows the least bias from SPIReS in simulating the spatial distribution of SCF climatology, achieving the highest R value of 0.87 and the highest SS value of 0.68. Additionally, it attains moderate accuracy in annual trend analysis. Overall, HMASR is the most suitable reanalysis dataset for SCF spatial simulation in the TP, benefiting from the direct assimilation of spectral unmixing algorithm derived SCF data from MODIS and Landsat satellites. GLDAS and CFSR are commendable for their spatial simulation accuracy of SCF, ranking just behind HMASR. However, their performance in annual trends is suboptimal, largely due to their poor representation of snowfall and temperature annual trends.~~

~~Conversely, ERA5 and ERA5L exhibit SCF overestimation across most of the TP, resulting in moderate SS values of 0.42 and 0.5 due to high RMSEs. Overestimated snowfall and underestimated temperature jointly contribute to the overestimation of SCF over most of the TP. Moreover, compared with snowfall, temperature-related physical processes have a more pronounced and widespread responsibility for SCF bias and the seasonal variation of SCF bias. Nevertheless, ERA5 and ERA5L show the best performance in annual trend simulations among the reanalysis datasets. The relatively good performance benefits from their accurate simulations of snowfall and temperature annual trends. JRA55, which overestimates SCF but performs well in annual trend, is more sensitive to the choice of SCF parameterization than to meteorological forcing factors. Moreover, its indirect assimilation of SD data does not effectively correct errors introduced by parameterization processing.~~

~~MERRA2, with the poorest spatial simulation indicated by the lowest STDR, R, and SS values, along with moderate CI values in annual trend simulation, ranks as the least effective reanalysis dataset for SCF simulation in the TP. This underperformance is attributed to errors in meteorological factors and a lack of snow data assimilation. CRAL demonstrates moderate accuracy in both spatial distribution and annual trend, which is consistent with its moderate performance in snowfall and temperature.~~

A three~~two~~-member combined of CFSR, GLDAS, and HMASR ~~HMASR and GLDAS~~ is optimal for the study of SCF spatial scales, while the combination of ERA5L, JRA55, HMASR,

ERA5, GLDAS, and CRAL ~~whereas a three-member combined of ERA5L, ERA5, and JRA55~~ is optimal for the study of annual trends.

These findings are crucial for selecting the most suitable reanalysis SCF datasets and gaining deeper insights into SCF variations and their controlling mechanisms on the TP. Reducing uncertainties within reanalysis SCF datasets stands as a pivotal stride toward refining climate models and prediction systems. Considering the significant impact of precipitation and temperature bias~~, along with snow assimilation~~, acquiring more precise meteorological forcing data ~~and snow observation data~~ is essential to further enhance the accuracy of reanalysis SCF simulations. Simultaneously, selecting more appropriate parameterization methods specific to reanalysis data models will contribute to improving dataset reliability. Optimizing simulations of snow cover on the TP will provide critical support for future climate change research and response strategies.

Conflicts of interest

The authors declared that they have no conflicts of interest to this work. We declare that we do not have any commercial or associative interest that represents a conflict of interest in connection with the work submitted.

Data Availability Statement

The SPIReS product used in this work is publicly available from http://ftp.snow.ucsb.edu. The TPMFD dataset are obtained from the National Tibetan Plateau Science Data Center (TPDC; https://cstr.cn/18406.11.Atmos.tpdc.300398.). All the reanalysis data are also acquired online: HMASR is obtained from on National Snow and Ice Data Center (NSIDC; https://doi.org/10.5067/HNAUGJQXSCVU). ERA5 and ERA5L data are downloaded from the Copernicus Climate Change Service Climate Date Store (CDS; https://doi.org/10.24381).

JRA55 and CFSR is downloaded from the NSF NCAR Research Data Archive (RDA; https://rda.ucar.edu). CRAL is obtained from the National Meteorological Information Center (CMA Meteorological Data Centre; https://data.cma.cn/en). MERRA2 and GLDAS-2.1 data is obtained from the NASA Goddard Earth Sciences Data and Information Service Center (GES DISC; https://disc.gsfc.nasa.gov/).~~publicly available and can be freely downloaded from the internet.~~

Acknowledgments

This research was supported by the National Science Fund for Distinguished Young Scholars (42025102), the Natural Science Foundation of Gansu province, China (21ZDKA0017), the National Natural Science Foundation of China (42375068, 42075061, and 42301142).

~~References~~

References

Adler, R. F., Huffman, G. J., Chang, A., Ferraro, R., Xie, P.-P., Janowiak, J., Rudolf, B., Schneider, U., Curtis, S., Bolvin, D., Gruber, A., Susskind, J., Arkin, P., and Nelkin, E.: The Version-2 Global Precipitation Climatology Project (GPCP) monthly precipitation analysis (1979–present), J. Hydrometeorol., 4, 1147–1167, https://doi.org/10.1175/1525-7541(2003)004<1147:TVGPCP>2.0.CO;2, 2003.

Andreadis, K. M. and Lettenmaier, D. P.: Assimilating remotely sensed snow observations into a macroscale hydrology model, Adv. Water Resour., 29, 872–886, https://doi.org/10.1016/j.advwatres.2005.08.004, 2006.

Bair, E. H., Stillinger, T., and Dozier, J.: Snow Property Inversion from Remote Sensing (SPIReS): a generalized multispectral unmixing approach with examples from MODIS and Landsat 8 OLI, IEEE Trans. Geosci. Remote Sens., 59, 7270–7284, https://doi.org/10.1109/TGRS.2020.3040328, 2021.

Bian, Q., Xu, Z., Zhao, L., Zhang, Y.-F., Zheng, H., Shi, C., Zhang, S., Xie, C., and Yang, Z.-L.: Evaluation and intercomparison of multiple snow water equivalent products over the Tibetan Plateau, J. Hydrometeorol., 20, 2043–2055, https://doi.org/10.1175/JHM-D-19-0011.1, 2019.

Brown, R. D. and Mote, P. W.: The response of Northern Hemisphere snow cover to a changing climate*, J. Clim., 22, 2124–2145, https://doi.org/10.1175/2008JCLI2665.1, 2009.

Cao, B., Gruber, S., Zheng, D., and Li, X.: The ERA5-Land soil temperature bias in permafrost regions, The Cryosphere, 14, 2581–2595, https://doi.org/10.5194/tc-14-2581-2020, 2020.

Danielson, J. J. and Gesch, D. B.: Global multi-resolution terrain elevation data 2010 (GMTED2010), https://doi.org/10.3133/ofr20111073, 2011.

de Rosnay, P., Balsamo, G., Albergel, C., Muñoz-Sabater, J., and Isaksen, L.: Initialisation of land surface variables for numerical weather prediction, Surv. Geophys., 35, 607–621, https://doi.org/10.1007/s10712-012-9207-x, 2014.

Deng, H., Pepin, N. C., and Chen, Y.: Changes of snowfall under warming in the Tibetan Plateau, J. Geophys. Res. ~~Atmospheres~~Atmos., 122, 7323–7341, https://doi.org/10.1002/2017JD026524, 2017.

Déry, S. J. and Yau, M. K.: Large-scale mass balance effects of blowing snow and surface sublimation, J. Geophys. Res. Atmos., 107, ACL 8-1-ACL 8-17, https://doi.org/10.1029/2001JD001251, 2002.

Ding, B., Yang, K., Qin, J., Wang, L., Chen, Y., and He, X.: The dependence of precipitation types on surface elevation and meteorological conditions and its parameterization, J. Hydrol., 513, 154–163, https://doi.org/10.1016/j.jhydrol.2014.03.038, 2014.

Dozier, J., Painter, T. H., Rittger, K., and Frew, J. E.: Time–space continuity of daily maps of fractional snow cover and albedo from MODIS, Adv. Water Resour., 31, 1515–1526, https://doi.org/10.1016/j.advwatres.2008.08.011, 2008.

Dutra, E., Kotlarski, S., Viterbo, P., Balsamo, G., Miranda, P. M. A., Schär, C., Bissolli, P., and Jonas, T.: Snow cover sensitivity to horizontal resolution, parameterizations, and atmospheric forcing in a land surface model, J. Geophys. Res. Atmos., 116, https://doi.org/10.1029/2011JD016061, 2011. –

Ek, M. B., Mitchell, K. E., Lin, Y., Rogers, E., Grunmann, P., Koren, V., Gayno, G., and Tarpley, J. D.: Implementation of Noah land surface model advances in the National Centers for Environmental Prediction operational mesoscale Eta model, J. Geophys. Res. Atmos., 108, 2002JD003296, https://doi.org/10.1029/2002JD003296, 2003.

Fujiwara, M., Wright, J. S., Manney, G. L., Gray, L. J., Anstey, J., Birner, T., Davis, S., Gerber, E. P., Harvey, V. L., Hegglin, M. I., Homeyer, C. R., Knox, J. A., Krüger, K., Lambert, A., Long, C. S., Martineau, P., Molod, A., Monge-Sanz, B. M., Santee, M. L., Tegtmeier, S., Chabrillat, S., Tan, D. G. H., Jackson, D. R., Polavarapu, S., Compo, G. P., Dragani, R., Ebisuzaki, W., Harada, Y., Kobayashi, C., McCarty, W., Onogi, K., Pawson, S., Simmons, A., Wargan, K., Whitaker, J. S., and Zou, C.-Z.: Introduction to the SPARC Reanalysis Intercomparison Project (S-RIP) and overview of the reanalysis systems, Atmos. Chem. Phys., 17, 1417–1452, https://doi.org/10.5194/acp-17-1417-2017, 2017.

Gelaro, R., McCarty, W., Suárez, M. J., Todling, R., Molod, A., Takacs, L., Randles, C. A., Darmenov, A., Bosilovich, M. G., Reichle, R., Wargan, K., Coy, L., Cullather, R., Draper, C., Akella, S., Buchard, V., Conaty, A., Silva, A. M. da, Gu, W., Kim, G.-K., Koster, R., Lucchesi, R., Merkova, D., Nielsen, J. E., Partyka, G., Pawson, S., Putman, W., Rienecker, M., Schubert, S. D., Sienkiewicz, M., and Zhao, B.: The Modern-Era Retrospective analysis for Research and Applications, version 2 (MERRA-2), J. Clim., 30, 5419–5454, https://doi.org/10.1175/JCLI-D-16-0758.1, 2017.

Hall, D. K., Riggs, G. A., Salomonson, V. V., DiGirolamo, N. E., and Bayr, K. J.: MODIS snow-cover products, Remote Sens. Environ., 83, 181–194, https://doi.org/10.1016/S0034-4257(02)00095-0, 2002.

Helfrich, S. R., McNamara, D., Ramsay, B. H., Baldwin, T., and Kasheta, T.: Enhancements to, and forthcoming developments in the Interactive Multisensor Snow and Ice Mapping System (IMS), Hydrol. Processes, 21, 1576–1586, https://doi.org/10.1002/hyp.6720, 2007.

Hernández-Henríquez, M. A., Déry, S. J., and Derksen, C.: Polar amplification and elevation-dependence in trends of Northern Hemisphere snow cover extent, 1971–2014, Environ. Res. Lett., 10, 044010, https://doi.org/10.1088/1748-9326/10/4/044010, 2015.

Hersbach, H., Bell, B., Berrisford, P., Hirahara, S., Horányi, A., Muñoz-Sabater, J., Nicolas, J., Peubey, C., Radu, R., Schepers, D., Simmons, A., Soci, C., Abdalla, S., Abellan, X., Balsamo, G., Bechtold, P., Biavati, G., Bidlot, J., Bonavita, M., Chiara, G., Dahlgren, P., Dee, D., Diamantakis, M., Dragani, R., Flemming, J., Forbes, R., Fuentes, M., Geer, A., Haimberger, L., Healy, S., Hogan, R. J., Hólm, E., Janisková, M., Keeley, S., Laloyaux, P., Lopez, P., Lupu, C., Radnoti, G., Rosnay, P., Rozum, I., Vamborg, F., Villaume, S., and Thépaut, J.: The ERA5 global reanalysis, Q. J. R. Meteorolog. Soc., 146, 1999–2049, https://doi.org/10.1002/qj.3803, 2020.

Huang, J., Zhou, X., Wu, G., Xu, X., Zhao, Q., Liu, Y., Duan, A., Xie, Y., Ma, Y., Zhao, P., Yang, S., Yang, K., Yang, H., Bian, J., Fu, Y., Ge, J., Liu, Y., Wu, Q., Yu, H., Wang, B., Bao, Q., and Qie, K.: Global climate impacts of land - surface and atmospheric processes over the Tibetan Plateau, Rev. Geophys., 61, e2022RG000771, https://doi.org/10.1029/2022RG000771, 2023.

Huffman, G. J., Adler, R. F., Morrissey, M. M., Bolvin, D. T., Curtis, S., Joyce, R., McGavock, B., and Susskind, J.: Global precipitation at one-degree daily resolution from multisatellite observations, J. Hydrometeorol., 2, 36–50, https://doi.org/10.1175/1525-7541(2001)002<0036:GPAODD>2.0.CO;2, 2001.

Immerzeel, W. W., Van Beek, L. P. H., and Bierkens, M. F. P.: Climate change will affect the Asian water towers, Science, 328, 1382–1385, https://doi.org/10.1126/science.1183188, 2010.

Jiang, Y., Chen, F., Gao, Y., He, C., Barlage, M., and Huang, W.: Assessment of uncertainty sources in snow cover simulation in the Tibetan Plateau, J. Geophys. Res. Atmos., 125, https://doi.org/10.1029/2020JD032674, 2020.

Jiang, Y., Yang, K., Qi, Y., Zhou, X., He, J., Lu, H., Li, X., Chen, Y., Li, X., Zhou, B., Mamtimin, A., Shao, C., Ma, X., Tian, J., and Zhou, J.: TPHiPr: a long-term (1979–2020) high-accuracy precipitation dataset (1 / 30°, daily) for the Third Pole region based on high-resolution atmospheric modeling and dense observations, Earth Syst. Sci. Data, 15, 621–638, https://doi.org/10.5194/essd-15-621-2023, 2023.

Kitoh, A. and Arakawa, O.: Reduction in the east–west contrast in water budget over the Tibetan Plateau under a future climate, Hydrol. Res. Lett., 10, 113–118, https://doi.org/10.3178/hrl.10.113, 2016.

Kobayashi, S., Ota, Y., Harada, Y., Ebita, A., Moriya, M., Onoda, H., Onogi, K., Kamahori, H., Kobayashi, C., Endo, H., Miyaoka, K., and Takahashi, K.: The JRA-55 Reanalysis: General Specifications and Basic Characteristics, J. Meteorolog. Soc. Jpn., 93, 5–48, https://doi.org/10.2151/jmsj.2015-001, 2015.

Koster, R. D., Suarez, M. J., Ducharne, A., Stieglitz, M., and Kumar, P.: A catchment-based approach to modeling land surface processes in a general circulation model: 1. Model structure, J. Geophys. Res. Atmos., 105, 24809–24822, https://doi.org/10.1029/2000JD900327, 2000.

Lehner, B., Verdin, K., and Jarvis, A.: New Global Hydrography Derived From Spaceborne Elevation Data, EoS Transactions, 89, 93–94, https://doi.org/10.1029/2008EO100001, 2008.

Lei, Y., Pan, J., Xiong, C., Jiang, L., and Shi, J.: Snow depth and snow cover over the Tibetan Plateau observed from space in against ERA5: matters of scale, Clim. Dyn., 60, 1523–1541, https://doi.org/10.1007/s00382-022-06376-0, 2023.

Li, Q., Yang, T., and Li, L.: Evaluation of snow depth and snow cover represented by multiple datasets over the Tianshan Mountains: Remote sensing, reanalysis, and simulation, Int. J. Climatol., 42, 4223–4239, https://doi.org/10.1002/joc.7459, 2022.

Liang, X., Jiang, L., Pan, Y., Shi, C., Liu, Z., and Zhou, Z.: A 10-Yr global land surface reanalysis interim dataset (CRA-Interim/Land): Implementation and preliminary evaluation, J. Meteorolog. Res., 34, 101–116, https://doi.org/10.1007/s13351-020-9083-0, 2020.

Lin, H. and Wu, Z.: Contribution of the autumn Tibetan Plateau snow cover to seasonal prediction of North American winter temperature, J. Clim., 24, 2801–2813, https://doi.org/10.1175/2010JCLI3889.1, 2011.

Liu, Y., Fang, Y., Li, D., and Margulis, S. A.: How well do global snow products characterize snow storage in High Mountain Asia?, Geophys. Res. Lett., 49, https://doi.org/10.1029/2022GL100082, 2022.

Liu, Y., Fang, Y., and Margulis, S. A.: Spatiotemporal distribution of seasonal snow water equivalent in High Mountain Asia from an 18-year Landsat–MODIS era snow reanalysis dataset, The Cryosphere, 15, 5261–5280, https://doi.org/10.5194/tc-15-5261-2021, 2021.

Liu, Z., Jiang, L., Shi, C., Zhang, T., Zhou, Z., Liao, J., Yao, S., Liu, J., Wang, M., Wang, H., Liang, X., Zhang, Z., Yao, Y., Zhu, T., Chen, Z., Xu, W., Cao, L., Jiang, H., and Hu, K.: CRA-40/Atmosphere—the first-generation

Chinese atmospheric reanalysis (1979–2018): System description and performance evaluation, J. Meteorolog. Res., 37, 1–19, https://doi.org/10.1007/s13351-023-2086-x, 2023.

Luo, J., Chen, H., and Zhou, B.: Comparison of Snowfall Variations over China Identified from Different Snowfall/Rainfall Discrimination Methods, J. Meteorol. Res., 34, 1114–1128, https://doi.org/10.1007/s13351-020-0004-z, 2020.

Lyu, M., Wen, M., and Wu, Z.: Possible contribution of the inter-annual Tibetan Plateau snow cover variation to the Madden-Julian oscillation convection variability, Int. J. Climatol., 38, 3787–3800, https://doi.org/10.1002/joc.5533, 2018.

Ma, Y., Ma, W., Zhong, L., Hu, Z., Li, M., Zhu, Z., Han, C., Wang, B., and Liu, X.: Monitoring and Modeling the Tibetan Plateau's climate system and its impact on East Asia, Sci. Rep., 7, 44574, https://doi.org/10.1038/srep44574, 2017.

Meng, J., Yang, R., Wei, H., Ek, M., Gayno, G., Xie, P., and Mitchell, K.: The land surface analysis in the NCEP climate forecast system reanalysis, J. Hydrometeorol., 13, 1621–1630, https://doi.org/10.1175/JHM-D-11-090.1, 2012.

Mortimer, C., Mudryk, L., Derksen, C., Luojus, K., Brown, R., Kelly, R., and Tedesco, M.: Evaluation of long-term Northern Hemisphere snow water equivalent products, The Cryosphere, 14, 1579–1594, https://doi.org/10.5194/tc-14-1579-2020, 2020.

Mudryk, L. R., Derksen, C., Kushner, P. J., and Brown, R.: Characterization of Northern Hemisphere snow water equivalent datasets, 1981–2010, J. Clim., 28, 8037–8051, https://doi.org/10.1175/JCLI-D-15-0229.1, 2015.

Muñoz-Sabater, J., Dutra, E., Agustí-Panareda, A., Albergel, C., Arduini, G., Balsamo, G., Boussetta, S., Choulga, M., Harrigan, S., Hersbach, H., Martens, B., Miralles, D. G., Piles, M., Rodríguez-Fernández, N. J., Zsoter, E., Buontempo, C., and Thépaut, J.-N.: ERA5-Land: a state-of-the-art global reanalysis dataset for land applications, Earth Syst. Sci. Data, 13, 4349–4383, https://doi.org/10.5194/essd-13-4349-2021, 2021.

Onogi, K., Tsutsui, J., Koide, H., Sakamoto, M., Kobayashi, S., Hatsushika, H., Matsumoto, T., Yamazaki, N., Kamahori, H., Takahashi, K., Kadokura, S., Wada, K., Kato, K., Oyama, R., Ose, T., Mannoji, N., and Taira, R.: The JRA-25 reanalysis, J. Meteorolog. Soc. Jpn., 85, 369–432, https://doi.org/10.2151/jmsj.85.369, 2007.

Orsolini, Y., Wegmann, M., Dutra, E., Liu, B., Balsamo, G., Yang, K., De Rosnay, P., Zhu, C., Wang, W., Senan, R., and Arduini, G.: Evaluation of snow depth and snow cover over the Tibetan Plateau in global reanalyses

using in situ and satellite remote sensing observations, The Cryosphere, 13, 2221–2239, https://doi.org/10.5194/tc-13-2221-2019, 2019.

Painter, T. H., Rittger, K., McKenzie, C., Slaughter, P., Davis, R. E., and Dozier, J.: Retrieval of subpixel snow covered area, grain size, and albedo from MODIS, Remote Sens. Environ., 113, 868–879, https://doi.org/10.1016/j.rse.2009.01.001, 2009.

Qiu, J.: China: The third pole, Nature, 454, 393–396, https://doi.org/10.1038/454393a, 2008.

Reichle, R. H., Draper, C. S., Liu, Q., Girotto, M., Mahanama, S. P. P., Koster, R. D., and Lannoy, G. J. M. D.: Assessment of MERRA-2 Land Surface Hydrology Estimates, J. Clim., 30, 2937–2960, https://doi.org/10.1175/JCLI-D-16-0720.1, 2017.

Rodell, M., Houser, P. R., Jambor, U., Gottschalck, J., Mitchell, K., Meng, C.-J., Arsenault, K., Cosgrove, B., Radakovich, J., Bosilovich, M., Entin, J. K., Walker, J. P., Lohmann, D., and Toll, D.: The global land data assimilation system, Bull. Am. Meteorol. Soc., 85, 381–394, https://doi.org/10.1175/BAMS-85-3-381, 2004.

Saha, S., Moorthi, S., Pan, H.-L., Wu, X., Wang, J., Nadiga, S., Tripp, P., Kistler, R., Woollen, J., Behringer, D., Liu, H., Stokes, D., Grumbine, R., Gayno, G., Wang, J., Hou, Y.-T., Chuang, H., Juang, H.-M. H., Sela, J., Iredell, M., Treadon, R., Kleist, D., Van Delst, P., Keyser, D., Derber, J., Ek, M., Meng, J., Wei, H., Yang, R., Lord, S., Van Den Dool, H., Kumar, A., Wang, W., Long, C., Chelliah, M., Xue, Y., Huang, B., Schemm, J.-K., Ebisuzaki, W., Lin, R., Xie, P., Chen, M., Zhou, S., Higgins, W., Zou, C.-Z., Liu, Q., Chen, Y., Han, Y., Cucurull, L., Reynolds, R. W., Rutledge, G., and Goldberg, M.: The NCEP climate forecast system reanalysis, Bull. Am. Meteorol. Soc., 91, 1015–1058, https://doi.org/10.1175/2010BAMS3001.1, 2010.

Saha, S., Moorthi, S., Wu, X., Wang, J., Nadiga, S., Tripp, P., Behringer, D., Hou, Y.-T., Chuang, H., Iredell, M., Ek, M., Meng, J., Yang, R., Mendez, M. P., Van Den Dool, H., Zhang, Q., Wang, W., Chen, M., and Becker, E.: The NCEP climate forecast system version 2, J. Clim., 27, 2185–2208, https://doi.org/10.1175/JCLI-D-12-00823.1, 2014.

Sato, N., Sellers, P. J., Randall, D. A., Schneider, E. K., Shukla, J., Kinter, J. L., Hou, Y.-T., and Albertazzi, E.: Effects of implementing the Simple Biosphere Model in a general circulation model, J. Atmos. Sci., 46, 2757–2782, https://doi.org/10.1175/1520-0469(1989)046<2757:EOITSB>2.0.CO;2, 1989.

Sellers, P. J., Mintz, Y., Sud, Y. C., and Dalcher, A.: A Simple Biosphere Model (SIB) for use within general circulation models, J. Atmos. Sci., 43, 505–531, https://doi.org/10.1175/1520-

0469(1986)043<0505:ASBMFU>2.0.CO;2, 1986.

Serquet, G., Marty, C., Dulex, J.-P., and Rebetez, M.: Seasonal trends and temperature dependence of the snowfall/precipitation-day ratio in Switzerland, Geophys. Res. Lett., 38, https://doi.org/10.1029/2011GL046976, 2011.

Sheffield, J., Goteti, G., and Wood, E. F.: Development of a 50-Year High-Resolution Global Dataset of Meteorological Forcings for Land Surface Modeling, J. Clim., 19, 3088–3111, https://doi.org/10.1175/JCLI3790.1, 2006.

Stillinger, T., Rittger, K., Raleigh, M. S., Michell, A., Davis, R. E., and Bair, E. H.: Landsat, MODIS, and VIIRS snow cover mapping algorithm performance as validated by airborne lidar datasets, The Cryosphere, 17, 567–590, https://doi.org/10.5194/tc-17-567-2023, 2023.

Sun, C., Walker, J. P., and Houser, P. R.: A methodology for snow data assimilation in a land surface model, J. Geophys. Res. Atmos., 109, 2003JD003765, https://doi.org/10.1029/2003JD003765, 2004.

Sun, S. and Xue, Y.: Implementing a new snow scheme in Simplified Simple Biosphere Model, Adv. Atmos. Sci., 18, 335–354, https://doi.org/10.1007/BF02919314, 2001.

Sun, S., Shi, C., Liang, X., Zhang, S., Gu, J., Han, S., Jiang, H., Xu, B., Yu, Q., Liang, Y., and Deng, S.: The Evaluation of Snow Depth Simulated by Different Land Surface Models in China Based on Station Observations, Sustainability, 15, 11284, https://doi.org/10.3390/su151411284, 2023.

Thackeray, C. W., Fletcher, C. G., Mudryk, L. R., and Derksen, C.: Quantifying the Uncertainty in Historical and Future Simulations of Northern Hemisphere Spring Snow Cover, J. Clim., 29, 8647–8663, https://doi.org/10.1175/JCLI-D-16-0341.1, 2016.

Vorkauf, M., Marty, C., Kahmen, A., and Hiltbrunner, E.: Past and future snowmelt trends in the Swiss Alps: the role of temperature and snowpack, Clim. Change, 165, 44, https://doi.org/10.1007/s10584-021-03027-x, 2021.

Wang, A. and Zeng, X.: Evaluation of multireanalysis products with in situ observations over the Tibetan Plateau, J. Geophys. Res. Atmospheres, 117, D05102, https://doi.org/10.1029/2011JD016553, 2012.

Wegmann, M., Orsolini, Y., Dutra, E., Bulygina, O., Sterin, A., and Brönnimann, S.: Eurasian snow depth in long-term climate reanalyses, The Cryosphere, 11, 923–935, https://doi.org/10.5194/tc-11-923-2017, 2017.

Xie, P. and Arkin, P. A.: Global precipitation: A 17-year monthly analysis based on gauge observations, satellite

estimates, and numerical model Outputs, Bull. Am. Meteorol. Soc., 78, 2539–2558, https://doi.org/10.1175/1520-0477(1997)078<2539:GPAYMA>2.0.CO;2, 1997.

Xie, P., Chen, M., Yang, S., Yatagai, A., Hayasaka, T., Fukushima, Y., and Liu, C.: A gauge-based analysis of daily precipitation over East Asia, J. Hydrometeorol., 8, 607–626, https://doi.org/10.1175/JHM583.1, 2007.

Xu, W., Ma, L., Ma, M., Zhang, H., and Yuan, W.: Spatial–temporal variability of snow cover and depth in the Qinghai–Tibetan Plateau, J. Clim., 30, 1521–1533, https://doi.org/10.1175/JCLI-D-15-0732.1, 2017.

Xu, X., Lu, C., Shi, X., and Gao, S.: World water tower: An atmospheric perspective, Geophys. Res. Lett., 35, L20815, https://doi.org/10.1029/2008GL035867, 2008.

Xue, Y., Sun, S., Kahan, D. S., and Jiao, Y.: Impact of parameterizations in snow physics and interface processes on the simulation of snow cover and runoff at several cold region sites, J. Geophys. Res. Atmos., 108, 2002JD003174, https://doi.org/10.1029/2002JD003174, 2003.

Yang, D., Ding, M., Dou, T., Han, W., Liu, W., Zhang, J., Du, Z., and Xiao, C.: On the Differences in Precipitation Type Between the Arctic, Antarctica and Tibetan Plateau, Front. Earth Sci., 9, https://doi.org/10.3389/feart.2021.607487, 2021.

Yang, K., Jiang, Z., Tang, W., He, J., Shao, C., Zhou, X., Lu, H., Chen, Y., Li, X., and Shi, J.: A high-resolution near-surface meteorological forcing dataset for the Third Pole region (TPMFD, 1979-2022), https://doi.org/10.11888/Atmos.tpdc.300398, 2023.

Yang, M., Wang, X., Pang, G., Wan, G., and Liu, Z.: The Tibetan Plateau cryosphere: Observations and model simulations for current status and recent changes, Earth Sci. Rev., 190, 353–369, https://doi.org/10.1016/j.earscirev.2018.12.018, 2019.

Yao, T., Thompson, L., Yang, W., Yu, W., Gao, Y., Guo, X., Yang, X., Duan, K., Zhao, H., Xu, B., Pu, J., Lu, A., Xiang, Y., Kattel, D. B., and Joswiak, D.: Different glacier status with atmospheric circulations in Tibetan Plateau and surroundings, Nat. Clim. Change, 2, 663–667, https://doi.org/10.1038/nclimate1580, 2012.

Yao, T., Xue, Y., Chen, D., Chen, F., Thompson, L., Cui, P., Koike, T., Lau, W. K.-M., Lettenmaier, D., Mosbrugger, V., Zhang, R., Xu, B., Dozier, J., Gillespie, T., Gu, Y., Kang, S., Piao, S., Sugimoto, S., Ueno, K., Wang, L., Wang, W., Zhang, F., Sheng, Y., Guo, W., Ailikun, Yang, X., Ma, Y., Shen, S. S. P., Su, Z., Chen, F., Liang, S., Liu, Y., Singh, V. P., Yang, K., Yang, D., Zhao, X., Qian, Y., Zhang, Y., and Li, Q.: Recent Third Pole's Rapid Warming Accompanies Cryospheric Melt and Water Cycle Intensification and Interactions between

Monsoon and Environment: Multidisciplinary Approach with Observations, Modeling, and Analysis, Bull. Am. Meteorol. Soc., 100, 423–444, https://doi.org/10.1175/BAMS-D-17-0057.1, 2019.

You, Q., Wu, F., Wang, H., Jiang, Z., Pepin, N., and Kang, S.: Projected changes in snow water equivalent over the Tibetan Plateau under global warming of 1.5° and 2°C, J. Clim., 33, 5141–5154, https://doi.org/10.1175/JCLI-D-19-0719.1, 2020a.

You, Q., Wu, T., Shen, L., Pepin, N., Zhang, L., Jiang, Z., Wu, Z., Kang, S., and AghaKouchak, A.: Review of snow cover variation over the Tibetan Plateau and its influence on the broad climate system, Earth Sci. Rev., 201, 103043, https://doi.org/10.1016/j.earscirev.2019.103043, 2020b.

Yu, L., Zhang, S., Bu, K., Yang, J., Yan, F., and Chang, L.: A review on snow data sets, Scientia Geographica Sinica, 33, 878–883, https://doi.org/10.13249/j.cnki.sgs.2013.07.878, 2013.

Zhang, F., Zhang, H., Hagen, S. C., Ye, M., Wang, D., Gui, D., Zeng, C., Tian, L., and Liu, J.: Snow cover and runoff modelling in a high mountain catchment with scarce data: effects of temperature and precipitation parameters, Hydrol. Processes, 29, 52–65, https://doi.org/10.1002/hyp.10125, 2015.

Zhang, H., Zhang, F., Che, T., Yan, W., and Ye, M.: Investigating the ability of multiple reanalysis datasets to simulate snow depth variability over mainland China from 1981 to 2018, J. Clim., 34, 9957–9972, https://doi.org/10.1175/JCLI-D-20-0804.1, 2021.

Zhang, H., Immerzeel, W. W., Zhang, F., De Kok, R. J., Chen, D., and Yan, W.: Snow cover persistence reverses the altitudinal patterns of warming above and below 5000 m on the Tibetan Plateau, Sci. Total Environ., 803, 149889, https://doi.org/10.1016/j.scitotenv.2021.149889, 2022.

Zhang, T.: Influence of the seasonal snow cover on the ground thermal regime: An overview, Rev. Geophys., 43, RG4002, https://doi.org/10.1029/2004RG000157, 2005.

Zhou, X., Yang, K., Ouyang, L., Wang, Y., Jiang, Y., Li, X., Chen, D., and Prein, A.: Added value of kilometer-scale modeling over the third pole region: a CORDEX-CPTP pilot study, Clim. Dyn., 57, 1673–1687, https://doi.org/10.1007/s00382-021-05653-8, 2021.~~Adler, R.F., Huffman, G.J., Chang, A., Ferraro, R., Xie, P.-P., Janowiak, J., Rudolf, B., Schneider, U., Curtis, S., Bolvin, D., Gruber, A., Susskind, J., Arkin, P., Nelkin, E., 2003. The Version-2 Global Precipitation Climatology Project (GPCP) monthly precipitation analysis (1979–present). J. Hydrometeorol. 4, 1147–1167. https://doi.org/10.1175/1525-7541(2003)004<1147:TVGPCP>2.0.CO;2~~

Zhu, X., Wu, T., Li, R., Wang, S., Hu, G., Wang, W., Qin, Y., and Yang, S.: Characteristics of the ratios of snow, rain and sleet to precipitation on the Qinghai-Tibet Plateau during 1961–2014, Quat. Int., 444, 137–150, https://doi.org/10.1016/j.quaint.2016.07.030, 2017.

(Zhu et al., 2017)Andreadis, K.M., Lettenmaier, D.P., 2006. Assimilating remotely sensed snow observations into a macroscale hydrology model. Adv. Water Resour. 29, 872–886. https://doi.org/10.1016/j.advwatres.2005.08.004

Bair, E.H., Stillinger, T., Dozier, J., 2021. Snow Property Inversion from Remote Sensing (SPIReS): a generalized multispectral unmixing approach with examples from MODIS and Landsat 8 OLI. IEEE Trans. Geosci. Remote Sens. 59, 7270–7284. https://doi.org/10.1109/TGRS.2020.3040328

Bian, Q., Xu, Z., Zhao, L., Zhang, Y. F., Zheng, H., Shi, C., Zhang, S., Xie, C., Yang, Z. L., 2019. Evaluation and intercomparison of multiple snow water equivalent products over the Tibetan Plateau. J. Hydrometeorol. 20, 2043–2055. https://doi.org/10.1175/JHM-D-19-0011.1

Brown, R.D., Brasnett, B., Robinson, D., 2003. Gridded North American monthly snow depth and snow water equivalent for GCM evaluation. Atmosphere-Ocean 41, 1–14. https://doi.org/10.3137/ao.410101

Brown, R.D., Mote, P.W., 2009. The response of Northern Hemisphere snow cover to a changing climate*. J. Clim. 22, 2124–2145. https://doi.org/10.1175/2008JCLI2665.1

Cui, T., Li, C., Tian, F., 2021. Evaluation of Temperature and Precipitation Simulations in CMIP6 Models Over the Tibetan Plateau. Earth Space Sci. 8, e2020EA001620. https://doi.org/10.1029/2020EA001620

Danielson, J.J., Gesch, D.B., 2011. Global multi-resolution terrain elevation data 2010 (GMTED2010) (No. 2011-1073), Open File Report. U.S. Geological Survey. https://doi.org/10.3133/ofr20111073

de Rosnay, P., Balsamo, G., Albergel, C., Muñoz-Sabater, J., Isaksen, L., 2014. Initialisation of land surface variables for numerical weather prediction. Surv. Geophys. 35, 607–621. https://doi.org/10.1007/s10712-012-9207-x

Deng, H., Pepin, N.C., Chen, Y., 2017. Changes of snowfall under warming in the Tibetan Plateau. J. Geophys. Res. Atmospheres 122, 7323–7341. https://doi.org/10.1002/2017JD026524

Déry, S.J., Yau, M.K., 2002. Large-scale mass balance effects of blowing snow and surface sublimation. J. Geophys. Res. Atmospheres 107, ACL 8-1–ACL 8-17. https://doi.org/10.1029/2001JD001251

Ding, B., Yang, K., Qin, J., Wang, L., Chen, Y., He, X., 2014. The dependence of precipitation types on surface elevation and meteorological conditions and its parameterization. J. Hydrol. 513, 154–163.

https://doi.org/10.1016/j.jhydrol.2014.03.038

Dozier, J., Painter, T.H., Rittger, K., Frew, J.E., 2008. Time–space continuity of daily maps of fractional snow cover and albedo from MODIS. Adv. Water Resour. 31, 1515–1526. https://doi.org/10.1016/j.advwatres.2008.08.011

Dutra, E., Kotlarski, S., Viterbo, P., Balsamo, G., Miranda, P.M.A., Schär, C., Bissolli, P., Jonas, T., 2011. Snow cover sensitivity to horizontal resolution, parameterizations, and atmospheric forcing in a land surface model. J. Geophys. Res. Atmospheres 116. https://doi.org/10.1029/2011JD016061

ECMWF, 2018. IFS Documentation CY45R1 Part IV : Physical processes, in: IFS Documentation CY45R1, IFS Documentation. ECMWF. https://doi.org/10.21957/4whwo8jw0

Ek, M.B., Mitchell, K.E., Lin, Y., Rogers, E., Grunmann, P., Koren, V., Gayno, G., Tarpley, J.D., 2003. Implementation of Noah land surface model advances in the National Centers for Environmental Prediction operational mesoscale Eta model. J. Geophys. Res. Atmospheres 108, 2002JD003296. https://doi.org/10.1029/2002JD003296

Fujiwara, M., Wright, J.S., Manney, G.L., Gray, L.J., Anstey, J., Birner, T., Davis, S., Gerber, E.P., Harvey, V.L., Hegglin, M.I., Homeyer, C.R., Knox, J.A., Krüger, K., Lambert, A., Long, C.S., Martineau, P., Molod, A., Monge-Sanz, B.M., Santee, M.L., Tegtmeier, S., Chabrillat, S., Tan, D.G.H., Jackson, D.R., Polavarapu, S., Compo, G.P., Dragani, R., Ebisuzaki, W., Harada, Y., Kobayashi, C., McCarty, W., Onogi, K., Pawson, S., Simmons, A., Wargan, K., Whitaker, J.S., Zou, C.-Z., 2017. Introduction to the SPARC Reanalysis Intercomparison Project (S-RIP) and overview of the reanalysis systems. Atmos. Chem. Phys. 17, 1417–1452. https://doi.org/10.5194/acp-17-1417-2017

Gelaro, R., McCarty, W., Suárez, M.J., Todling, R., Molod, A., Takacs, L., Randles, C.A., Darmenov, A., Bosilovich, M.G., Reichle, R., Wargan, K., Coy, L., Cullather, R., Draper, C., Akella, S., Buchard, V., Conaty, A., Silva, A.M. da, Gu, W., Kim, G.-K., Koster, R., Lucchesi, R., Merkova, D., Nielsen, J.E., Partyka, G., Pawson, S., Putman, W., Rienecker, M., Schubert, S.D., Sienkiewicz, M., Zhao, B., 2017. The Modern-Era Retrospective analysis for Research and Applications, version 2 (MERRA-2). J. Clim. 30, 5419–5454. https://doi.org/10.1175/JCLI-D-16-0758.1

Hall, D.K., Riggs, G.A., Salomonson, V.V., DiGirolamo, N.E., Bayr, K.J., 2002. MODIS snow-cover products. Remote Sens. Environ. 83, 181–194. https://doi.org/10.1016/S0034-4257(02)00095-0

Helfrich, S.R., McNamara, D., Ramsay, B.H., Baldwin, T., Kasheta, T., 2007. Enhancements to, and forthcoming developments in the Interactive Multisensor Snow and Ice Mapping System (IMS). Hydrol. Process. 21, 1576–1586. https://doi.org/10.1002/hyp.6720

Hernández Henríquez, M.A., Déry, S.J., Derksen, C., 2015. Polar amplification and elevation dependence in trends of Northern Hemisphere snow cover extent, 1971 2014. Environ. Res. Lett. 10, 044010. https://doi.org/10.1088/1748-9326/10/4/044010

Hersbach, H., Bell, B., Berrisford, P., Hirahara, S., Horányi, A., Muñoz Sabater, J., Nicolas, J., Peubey, C., Radu, R., Schepers, D., Simmons, A., Soci, C., Abdalla, S., Abellan, X., Balsamo, G., Bechtold, P., Biavati, G., Bidlot, J., Bonavita, M., Chiara, G., Dahlgren, P., Dee, D., Diamantakis, M., Dragani, R., Flemming, J., Forbes, R., Fuentes, M., Geer, A., Haimberger, L., Healy, S., Hogan, R.J., Hólm, E., Janisková, M., Keeley, S., Laloyaux, P., Lopez, P., Lupu, C., Radnoti, G., Rosnay, P., Rozum, I., Vamborg, F., Villaume, S., Thépaut, J., 2020. The ERA5 global reanalysis. Q. J. R. Meteorol. Soc. 146, 1999–2049. https://doi.org/10.1002/qj.3803

Huang, J., Zhou, X., Wu, G., Xu, X., Zhao, Q., Liu, Yimin, Duan, A., Xie, Y., Ma, Y., Zhao, P., Yang, S., Yang, K., Yang, H., Bian, J., Fu, Y., Ge, J., Liu, Yuzhi, Wu, Q., Yu, H., Wang, B., Bao, Q., Qie, K., 2023. Global climate impacts of land–surface and atmospheric processes over the Tibetan Plateau. Rev. Geophys. 61, e2022RG000771. https://doi.org/10.1029/2022RG000771

Huffman, G.J., Adler, R.F., Morrissey, M.M., Bolvin, D.T., Curtis, S., Joyce, R., McGavock, B., Susskind, J., 2001. Global precipitation at one-degree daily resolution from multisatellite observations. J. Hydrometeorol. 2, 36–50. https://doi.org/10.1175/1525-7541(2001)002<0036:GPAODD>2.0.CO;2

Immerzeel, W.W., Van Beek, L.P.H., Bierkens, M.F.P., 2010. Climate change will affect the Asian water towers. Science 328, 1382–1385. https://doi.org/10.1126/science.1183188

Jiang, Y., Chen, F., Gao, Y., He, C., Barlage, M., Huang, W., 2020. Assessment of uncertainty sources in snow cover simulation in the Tibetan Plateau. J. Geophys. Res. Atmospheres 125. https://doi.org/10.1029/2020JD032674

Jiang, Y., Yang, K., Qi, Y., Zhou, X., He, J., Lu, H., Li, Xin, Chen, Y., Li, Xiaodong, Zhou, B., Mamtimin, A., Shao, C., Ma, X., Tian, J., Zhou, J., 2023. TPHiPr: a long-term (1979–2020) high-accuracy precipitation dataset (1 / 30°, daily) for the Third Pole region based on high-resolution atmospheric modeling and dense observations. Earth Syst. Sci. Data 15, 621–638. https://doi.org/10.5194/essd-15-621-2023

Kendall, M.G., 1975. Rank Correlation Methods. J. Inst. Actuar. 75, 140–141. https://doi.org/10.1017/S0020268100013019

Kitoh, A., Arakawa, O., 2016. Reduction in the east–west contrast in water budget over the Tibetan Plateau under a future climate. Hydrol. Res. Lett. 10, 113–118. https://doi.org/10.3178/hrl.10.113

Kobayashi, S., Ota, Y., Harada, Y., Ebita, A., Moriya, M., Onoda, H., Onogi, K., Kamahori, H., Kobayashi, C., Endo, H., Miyaoka, K., Takahashi, K., 2015. The JRA-55 Reanalysis: General Specifications and Basic Characteristics. J. Meteorol. Soc. Jpn. Ser II 93, 5–48. https://doi.org/10.2151/jmsj.2015-001

Koster, R.D., Suarez, M.J., Ducharne, A., Stieglitz, M., Kumar, P., 2000. A catchment-based approach to modeling land surface processes in a general circulation model: 1. Model structure. J. Geophys. Res. Atmospheres 105, 24809–24822. https://doi.org/10.1029/2000JD900327

Lehner, B., Verdin, K., Jarvis, A., 2008. New Global Hydrography Derived From Spaceborne Elevation Data. Eos Trans. Am. Geophys. Union 89, 93–94. https://doi.org/10.1029/2008EO100001

Lei, Y., Pan, J., Xiong, C., Jiang, L., Shi, J., 2023. Snow depth and snow cover over the Tibetan Plateau observed from space in against ERA5: matters of scale. Clim. Dyn. 60, 1523–1541. https://doi.org/10.1007/s00382-022-06376-0

Li, Q., Yang, T., Li, L., 2022. Evaluation of snow depth and snow cover represented by multiple datasets over the Tianshan Mountains: Remote sensing, reanalysis, and simulation. Int. J. Climatol. 42, 4223–4239. https://doi.org/10.1002/joc.7459

Liang, X., Jiang, L., Pan, Y., Shi, C., Liu, Z., Zhou, Z., 2020. A 10-Yr global land surface reanalysis interim dataset (CRA-Interim/Land): Implementation and preliminary evaluation. J. Meteorol. Res. 34, 101–116. https://doi.org/10.1007/s13351-020-9083-0

Lin, H., Wu, Z., 2011. Contribution of the autumn Tibetan Plateau snow cover to seasonal prediction of North American winter temperature. J. Clim. 24, 2801–2813. https://doi.org/10.1175/2010JCLI3889.1

Liu, Y., Fang, Y., Li, D., Margulis, S.A., 2022. How well do global snow products characterize snow storage in High Mountain Asia? Geophys. Res. Lett. 49. https://doi.org/10.1029/2022GL100082

Liu, Y., Fang, Y., Margulis, S.A., 2021. Spatiotemporal distribution of seasonal snow water equivalent in High Mountain Asia from an 18-year Landsat–MODIS era snow reanalysis dataset. The Cryosphere 15, 5261–5280. https://doi.org/10.5194/tc-15-5261-2021

Liu, Z., Jiang, L., Shi, C., Zhang, T., Zhou, Z., Liao, J., Yao, S., Liu, J., Wang, M., Wang, H., Liang, X., Zhang, Z., Yao, Y., Zhu, T., Chen, Z., Xu, W., Cao, L., Jiang, H., Hu, K., 2023. CRA-40/Atmosphere—the first-generation Chinese atmospheric reanalysis (1979–2018): System description and performance evaluation. J. Meteorol. Res. 37, 1–19. https://doi.org/10.1007/s13351-023-2086-x

Luo, J., Chen, H., Zhou, B., 2020. Comparison of Snowfall Variations over China Identified from Different Snowfall/Rainfall Discrimination Methods. J. Meteorol. Res. 34, 1114–1128. https://doi.org/10.1007/s13351-020-0004-z

Lyu, M., Wen, M., Wu, Z., 2018. Possible contribution of the inter-annual Tibetan Plateau snow cover variation to the Madden Julian oscillation convection variability. Int. J. Climatol. 38, 3787–3800. https://doi.org/10.1002/joc.5533

Magnusson, J., Winstral, A., Stordal, A.S., Essery, R., Jonas, T., 2017. Improving physically based snow simulations by assimilating snow depths using the particle filter. Water Resour. Res. 53, 1125–1143. https://doi.org/10.1002/2016WR019092

Ma, Y., Ma, W., Zhong, L., Hu, Z., Li, M., Zhu, Z., Han, C., Wang, B., Liu, X., 2017. Monitoring and Modeling the Tibetan Plateau's climate system and its impact on East Asia. Sci. Rep. 7, 44574. https://doi.org/10.1038/srep44574

Ma, Y., Wang, B., Chen, X., Zhong, L., Hu, Z., Ma, W., Han, C., Li, M., 2022. Strengthening the three-dimensional comprehensive observation system of multi-layer interaction on the Tibetan Plateau to cope with the warming and wetting trend. Atmospheric Ocean. Sci. Lett. 15, 100224. https://doi.org/10.1016/j.aosl.2022.100224

Magnusson, J., Winstral, A., Stordal, A.S., Essery, R., Jonas, T., 2017. Improving physically based snow simulations by assimilating snow depths using the particle filter. Water Resour. Res. 53, 1125–1143. https://doi.org/10.1002/2016WR019092

Mann, H.B., 1945. Nonparametric tests against trend. Econometrica 13, 245–259. https://doi.org/10.2307/1907187

Meng, J., Yang, R., Wei, H., Ek, M., Gayno, G., Xie, P., Mitchell, K., 2012. The land surface analysis in the NCEP climate forecast system reanalysis. J. Hydrometeorol. 13, 1621–1630. https://doi.org/10.1175/JHM-D-11-090.1

Mortimer, C., Mudryk, L., Derksen, C., Luojus, K., Brown, R., Kelly, R., Tedesco, M., 2020. Evaluation of long-term Northern Hemisphere snow water equivalent products. The Cryosphere 14, 1579–1594. https://doi.org/10.5194/tc-14-1579-2020

Mudryk, L.R., Derksen, C., Kushner, P.J., Brown, R., 2015. Characterization of Northern Hemisphere snow water equivalent datasets, 1981–2010. J. Clim. 28, 8037–8051. https://doi.org/10.1175/JCLI-D-15-0229.1

Muñoz-Sabater, J., Dutra, E., Agustí-Panareda, A., Albergel, C., Arduini, G., Balsamo, G., Boussetta, S., Choulga, M., Harrigan, S., Hersbach, H., Martens, B., Miralles, D.G., Piles, M., Rodríguez-Fernández, N.J., Zsoter, E., Buontempo, C., Thépaut, J.-N., 2021. ERA5-Land: a state-of-the-art global reanalysis dataset for land applications. Earth Syst. Sci. Data 13, 4349–4383. https://doi.org/10.5194/essd-13-4349-2021

Onogi, K., Tsutsui, J., Koide, H., Sakamoto, M., Kobayashi, S., Hatsushika, H., Matsumoto, T., Yamazaki, N., Kamahori, H., Takahashi, K., Kadokura, S., Wada, K., Kato, K., Oyama, R., Ose, T., Mannoji, N., Taira, R., 2007. The JRA-25 reanalysis. J. Meteorol. Soc. Jpn. 85, 369–432. https://doi.org/10.2151/jmsj.85.369

Orsolini, Y., Wegmann, M., Dutra, E., Liu, B., Balsamo, G., Yang, K., De Rosnay, P., Zhu, C., Wang, W., Senan, R., Arduini, G., 2019. Evaluation of snow depth and snow cover over the Tibetan Plateau in global reanalysis using in situ and satellite remote sensing observations. The Cryosphere 13, 2221–2239. https://doi.org/10.5194/tc-13-2221-2019

Painter, T.H., Rittger, K., McKenzie, C., Slaughter, P., Davis, R.E., Dozier, J., 2009. Retrieval of subpixel snow covered area, grain size, and albedo from MODIS. Remote Sens. Environ. 113, 868–879. https://doi.org/10.1016/j.rse.2009.01.001

Qiu, J., 2008. China: The third pole. Nature 454, 393–396. https://doi.org/10.1038/454393a

Reichle, R.H., Draper, C.S., Liu, Q., Girotto, M., Mahanama, S.P.P., Koster, R.D., Lannoy, G.J.M.D., 2017. Assessment of MERRA-2 Land Surface Hydrology Estimates. J. Clim. 30, 2937–2960. https://doi.org/10.1175/JCLI-D-16-0720.1

Rodell, M., Houser, P.R., Jambor, U., Gottschalck, J., Mitchell, K., Meng, C. J., Arsenault, K., Cosgrove, B., Radakovich, J., Bosilovich, M., Entin, J.K., Walker, J.P., Lohmann, D., Toll, D., 2004. The global land data assimilation system. Bull. Am. Meteorol. Soc. 85, 381–394. https://doi.org/10.1175/BAMS-85-3-381

Saha, S., Moorthi, S., Pan, H.-L., Wu, X., Wang, Jiande, Nadiga, S., Tripp, P., Kistler, R., Woollen, J., Behringer, D., Liu, H., Stokes, D., Grumbine, R., Gayno, G., Wang, Jun, Hou, Y. T., Chuang, H., Juang, H. M.H., Sela, J., Iredell, M., Treadon, R., Kleist, D., Van Delst, P., Keyser, D., Derber, J., Ek, M., Meng, J., Wei, H., Yang, R., Lord, S., Van Den Dool, H., Kumar, A., Wang, W., Long, C., Chelliah, M., Xue, Y., Huang, B., Schemm, J.-K., Ebisuzaki, W., Lin, R., Xie, P., Chen, M., Zhou, S., Higgins, W., Zou, C.-Z., Liu, Q., Chen, Y., Han, Y., Cucurull, L., Reynolds,

R.W., Rutledge, G., Goldberg, M., 2010. The NCEP climate forecast system reanalysis. Bull. Am. Meteorol. Soc. 91, 1015–1058. https://doi.org/10.1175/2010BAMS3001.1

Saha, S., Moorthi, S., Wu, X., Wang, J., Nadiga, S., Tripp, P., Behringer, D., Hou, Y. T., Chuang, H., Iredell, M., Ek, M., Meng, J., Yang, R., Mendez, M.P., Van Den Dool, H., Zhang, Q., Wang, W., Chen, M., Becker, E., 2014. The NCEP climate forecast system version 2. J. Clim. 27, 2185–2208. https://doi.org/10.1175/JCLI-D-12-00823.1

Sato, N., Sellers, P.J., Randall, D.A., Schneider, E.K., Shukla, J., Kinter, J.L., Hou, Y.-T., Albertazzi, E., 1989. Effects of implementing the Simple Biosphere Model in a general circulation model. J. Atmospheric Sci. 46, 2757–2782. https://doi.org/10.1175/1520-0469(1989)046<2757:EOITSB>2.0.CO;2

Sellers, P.J., Mintz, Y., Sud, Y.C., Dalcher, A., 1986. A Simple Biosphere Model (SIB) for use within general circulation models. J. Atmospheric Sci. 43, 505–531. https://doi.org/10.1175/1520-0469(1986)043<0505:ASBMFU>2.0.CO;2

Serquet, G., Marty, C., Dulex, J. P., Rebetez, M., 2011. Seasonal trends and temperature dependence of the snowfall/precipitation-day ratio in Switzerland. Geophys. Res. Lett. 38. https://doi.org/10.1029/2011GL046976

Sheffield, J., Goteti, G., Wood, E.F., 2006. Development of a 50-Year High-Resolution Global Dataset of Meteorological Forcings for Land Surface Modeling. J. Clim. 19, 3088–3111. https://doi.org/10.1175/JCLI3790.1

Stillinger, T., Rittger, K., Raleigh, M.S., Michell, A., Davis, R.E., Bair, E.H., 2023. Landsat, MODIS, and VIIRS snow cover mapping algorithm performance as validated by airborne lidar datasets. The Cryosphere 17, 567–590. https://doi.org/10.5194/tc-17-567-2023

Sun, C., Walker, J.P., Houser, P.R., 2004. A methodology for snow data assimilation in a land surface model. J. Geophys. Res. Atmospheres 109, 2003JD003765. https://doi.org/10.1029/2003JD003765

Sun, S., Xue, Y., 2001. Implementing a new snow scheme in Simplified Simple Biosphere Model. Adv. Atmospheric Sci. 18, 335–354. https://doi.org/10.1007/BF02919314

Taylor, K.E., 2001. Summarizing multiple aspects of model performance in a single diagram. J. Geophys. Res. Atmospheres 106, 7183–7192. https://doi.org/10.1029/2000JD900719

Thackeray, C.W., Fletcher, C.G., Mudryk, L.R., Derksen, C., 2016. Quantifying the Uncertainty in Historical and Future Simulations of Northern Hemisphere Spring Snow Cover. J. Clim. 29, 8647–8663. https://doi.org/10.1175/JCLI-D-16-0341.1

Vorkauf, M., Marty, C., Kahmen, A., Hiltbrunner, E., 2021. Past and future snowmelt trends in the Swiss Alps: the

role of temperature and snowpack. Clim. Change 165, 44. https://doi.org/10.1007/s10584-021-03027-x

Wang, A., Zeng, X., 2012. Evaluation of multireanalysis products with in situ observations over the Tibetan Plateau. J. Geophys. Res. Atmospheres 117, D05102. https://doi.org/10.1029/2011JD016553

Wegmann, M., Orsolini, Y., Dutra, E., Bulygina, O., Sterin, A., Brönnimann, S., 2017. Eurasian snow depth in long-term climate reanalyses. The Cryosphere 11, 923–935. https://doi.org/10.5194/tc-11-923-2017

Xie, P., Arkin, P.A., 1997. Global precipitation: A 17-year monthly analysis based on gauge observations, satellite estimates, and numerical model Outputs. Bull. Am. Meteorol. Soc. 78, 2539–2558. https://doi.org/10.1175/1520-0477(1997)078<2539:GPAYMA>2.0.CO;2

Xie, P., Chen, M., Yang, S., Yatagai, A., Hayasaka, T., Fukushima, Y., Liu, C., 2007. A gauge-based analysis of daily precipitation over East Asia. J. Hydrometeorol. 8, 607–626. https://doi.org/10.1175/JHM583.1

Xu, W., Ma, L., Ma, M., Zhang, H., Yuan, W., 2017. Spatial–temporal variability of snow cover and depth in the Qinghai–Tibetan Plateau. J. Clim. 30, 1521–1533. https://doi.org/10.1175/JCLI-D-15-0732.1

Xu, X., Lu, C., Shi, X., Gao, S., 2008. World water tower: An atmospheric perspective. Geophys. Res. Lett. 35, L20815. https://doi.org/10.1029/2008GL035867

Xue, Y., Sun, S., Kahan, D.S., Jiao, Y., 2003. Impact of parameterizations in snow physics and interface processes on the simulation of snow cover and runoff at several cold region sites. J. Geophys. Res. Atmospheres 108, 2002JD003174. https://doi.org/10.1029/2002JD003174

Yang, D., Ding, M., Dou, T., Han, W., Liu, W., Zhang, J., Du, Z., Xiao, C., 2021. On the Differences in Precipitation Type Between the Arctic, Antarctica and Tibetan Plateau. Front. Earth Sci. 9. https://doi.org/10.3389/feart.2021.607487

Yang, K., Jiang, Z., Tang, W., He, J., Shao, C., Zhou, X., Lu, H., Chen, Y., Li, X., Shi, J., 2023. A high resolution near surface meteorological forcing dataset for the Third Pole region (TPMFD, 1979-2022). Natl. Tibet. Plateau Data Cent. https://doi.org/10.11888/Atmos.tpdc.300398

Yang, M., Wang, X., Pang, G., Wan, G., Liu, Z., 2019. The Tibetan Plateau cryosphere: Observations and model simulations for current status and recent changes. Earth-Sci. Rev. 190, 353–369. https://doi.org/10.1016/j.earscirev.2018.12.018

Yao, T., Thompson, L., Yang, W., Yu, W., Gao, Y., Guo, X., Yang, X., Duan, K., Zhao, H., Xu, B., Pu, J., Lu, A., Xiang, Y., Kattel, D.B., Joswiak, D., 2012. Different glacier status with atmospheric circulations in Tibetan Plateau

and surroundings. Nat. Clim. Change 2, 663–667. https://doi.org/10.1038/nclimate1580

Yao, T., Xue, Y., Chen, D., Chen, Fahu, Thompson, L., Cui, P., Koike, T., Lau, W.K. M., Lettenmaier, D., Mosbrugger, V., Zhang, R., Xu, B., Dozier, J., Gillespie, T., Gu, Y., Kang, S., Piao, S., Sugimoto, S., Ueno, K., Wang, L., Wang, W., Zhang, F., Sheng, Y., Guo, W., Ailikun, Yang, X., Ma, Y., Shen, S.S.P., Su, Z., Chen, Fei, Liang, S., Liu, Y., Singh, V.P., Yang, K., Yang, D., Zhao, X., Qian, Y., Zhang, Y., Li, Q., 2019. Recent Third Pole's Rapid Warming Accompanies Cryospheric Melt and Water Cycle Intensification and Interactions between Monsoon and Environment: Multidisciplinary Approach with Observations, Modeling, and Analysis. Bull. Am. Meteorol. Soc. 100, 423–444. https://doi.org/10.1175/BAMS-D-17-0057.1

You, Q., Wu, F., Wang, H., Jiang, Z., Pepin, N., Kang, S., 2020a. Projected changes in snow water equivalent over the Tibetan Plateau under global warming of 1.5° and 2°C. J. Clim. 33, 5141–5154. https://doi.org/10.1175/JCLI-D-19-0719.1

You, Q., Wu, T., Shen, L., Pepin, N., Zhang, L., Jiang, Z., Wu, Z., Kang, S., AghaKouchak, A., 2020b. Review of snow cover variation over the Tibetan Plateau and its influence on the broad climate system. Earth Sci. Rev. 201, 103043. https://doi.org/10.1016/j.earscirev.2019.103043

Yu, L., Zhang, S., Bu, K., Yang, J., Yan, F., Chang, L., 2013. A review on snow data sets. Sci. Geogr. Sin. 33, 878–883. https://doi.org/10.13249/j.cnki.sgs.2013.07.878

Zhang, F., Zhang, H., Hagen, S.C., Ye, M., Wang, D., Gui, D., Zeng, C., Tian, L., Liu, J., 2015. Snow cover and runoff modelling in a high mountain catchment with scarce data: effects of temperature and precipitation parameters. Hydrol. Process. 29, 52–65. https://doi.org/10.1002/hyp.10125

Zhang, H., Immerzeel, W.W., Zhang, F., De Kok, R.J., Chen, D., Yan, W., 2022. Snow cover persistence reverses the altitudinal patterns of warming above and below 5000 m on the Tibetan Plateau. Sci. Total Environ. 803, 149889. https://doi.org/10.1016/j.scitotenv.2021.149889

Zhang, H., Zhang, F., Che, T., Yan, W., Ye, M., 2021. Investigating the ability of multiple reanalysis datasets to simulate snow depth variability over mainland China from 1981 to 2018. J. Clim. 34, 9957–9972. https://doi.org/10.1175/JCLI-D-20-0804.1

Zhang, T., 2005. Influence of the seasonal snow cover on the ground thermal regime: An overview. Rev. Geophys. 43, RG4002. https://doi.org/10.1029/2004RG000157

Zhou, X., Yang, K., Ouyang, L., Wang, Y., Jiang, Y., Li, X., Chen, D., Prein, A., 2021. Added value of kilometer-

scale modeling over the third pole region: a CORDEX-CPTP pilot study. Clim. Dyn. 57, 1673–1687. https://doi.org/10.1007/s00382-021-05653-8

Zhu, X., Wu, T., Li, R., Wang, S., Hu, G., Wang, W., Qin, Y., Yang, S., 2017. Characteristics of the ratios of snow, rain and sleet to precipitation on the Qinghai-Tibet Plateau during 1961–2014. Quat. Int., Third Pole: The Last 20,000 Years - Part 2 444, 137–150. https://doi.org/10.1016/j.quaint.2016.07.030